Journal of Sound and Vibration (1999) **226**(2), 253–284
Article No. jsvi.1999.2299, available online at http://www.idealibrary.com on IDEAL®

THERMAL ANALOGY IN WAVE ENERGY TRANSFER: THEORETICAL AND EXPERIMENTAL ANALYSIS

A. CARCATERRA

Instituto Nazionale di Studi ed Esperienze di Architettura Navale, INSEAN, Via di Vallerano, 139, 00128, Rome, Italy

AND

L. ADAMO

Department of Mechanics and Aeronautics, University 'La Sapienza', Via Eudossiana 18, Rome, Italy

(*Received* 2 *December* 1997, *and in final form* 29 *March* 1999)

In this paper a theoretical and experimental analysis of the wave energy transmission in structures is proposed, aimed at introducing a new point of view about energy exchange in dynamical systems. A systematic asymptotic analysis, based on the concept of wavelength scale effect, is developed, in which a simultaneous time- and space-average energy along the structure is considered. The analytical approach highlights different scale laws in the energy transmission mechanism. The μ parameter, related to the ratio between a characteristic space-average length and the wavelength, controls this characteristic scale. In the small-scale transmission range ($\mu < 1$), a vibration conductivity principle fails for every type of considered structure. On the other hand, in the large-scale range ($\mu \gg 1$), an asymptotic thermal energy behaviour is found for one-dimensional systems. The plate energy does not indeed obey a thermal law. A physical explanation of these different behaviours is proposed and two types of basic energy interactions between waves are identified, leading to different energy contributions: the *coincident wave energy* and the *interference wave energy*, with totally different asymptotic features. In fact, the coincident wave energy asymptotically tends to satisfy the energy balance in a thermal form over the μ large-scale range. The interference energy indeed exhibits a complex behaviour: only part of its non-thermal contribution asymptotically vanishes, but another persists even in the large μ scale range.

1. INTRODUCTION

The problem of energy transmission in dynamical systems is important from a practical and theoretical point of view. When dealing with high-frequency dynamics, the standard methods of analysis based upon discretization techniques, fail. This is not only due to the computational cost that extends over reasonable limits, but also because the analysis reliability becomes in-significant due to the

0022-460X/99/370253 + 32 $30.00/0

uncertainties in the model parameters [1–3]. High-frequency dynamics involves nowadays a wide class of engineering applications. Structure-borne sound transmission problems are encountered in ship, aircraft and car design due to the requirements of weight reduction, better economy and increasing power set up on board (high-speed marine vehicles, jet aircrafts, rockets, etc.).

In this field, statistical energy analysis (SEA) [4] is at present the most widely acknowledged contribution. Based on the thermal exchange of mechanical energy among coupled dynamic systems, SEA provides information on the stored and the dissipated energy and on the transmitted power between modal subsystems.

In spite of the simplicity of this energetic formulation, which makes it particularly attractive, research on providing a solid theoretical basis of the SEA instances has required, and still requires, much attention by the scientific community. Although some relevant studies [5–9] have been developed on this topic and some points begin to be firm, the problem is still far from being definitely solved and free from controversies [6, 10–12].

In these last 10 years, several methods have been developed to meet new requirements. A large part of them, at least in the beginning, have been inspired by SEA thermal assumptions [13–15]. In these methods, extension of the original SEA statements is made. While in SEA the energy transmission between complex structures of finite size is considered, in the new approaches the same relationships are directly translated into differential form. In the rest of this paper, the common idea of these approaches in called the thermal analogy or vibration conductivity principle.

It is reasonable that all the doubts and uncertainties affecting the sphere of SEA have been transferred to the thermal analogy, with the aggravating circumstance that the local formulation posing totally new problems, that pass beyond the critical SEA limitations.

Other proposed approaches are indeed not conductivity based, even if they involve energy concepts [16–22]. Finally other methods, not involving energy concepts, have been recently proposed for high-frequency dynamics [23].

After the initial statement of the vibration conductivity was posed [13–15], in which the thermal energy transmission was assumed rather than demonstrated, the attention of researchers turned to a more strict derivation of the thermal analogy [24–29].

Unfortunately, their analyses did not always reach the same conclusions. This is in part comprehensible due to the complexity of the problem, which has led authors to use different simplified assumptions. On the other hand, different definitions of the energy variable are employed in deriving the governing equations. Moreover, little experimental work on the subject has been performed: the few experiments performed, although interesting [30, 31], did not have the goal of confirming or rejecting the thermal analysis, but rather were aimed to apply the thermal analogy to practical engineering problems.

The aim of the present work is to reconsider the thorny but fascinating problem of the vibration conductivity in the light of the wavelength scale effect. The basic idea is that the wave energy transmission is dominated by the ratio between a characteristic length d of the system and the characteristic wavelength λ generated

by the excitation. More precisely, the non-dimensional value of the ratio $\mu = d/\lambda$ seems to separate two different energy rate conditions: the same and the large μ scale regions. The effects of μ variations on the law of energy transmission is systematically investigated for one- and two-dimensional continuous waveguides. The main results concern the asymptotic analysis ($\mu \to \infty$) of the power flow. It will be shown that the power flow tends, for one-dimensional structures, to be asymptotically thermal. Instead, the two-dimensional problem has two main power flow components: the first is analogous to the one-dimensional case but the second has a completely different nature, whose characteristics are investigated. Experiments, performed using a laser technique, both on beams and plates, confirm the theoretical predictions, and the description and the interpretation of the results are discussed in the final part of the paper.

2. ENERGY BALANCE EQUATION AND CONSTITUTIVE RELATIONSHIPS

The Poynting vector is defined as [29, 32]

$$\mathbf{I} = \boldsymbol{\sigma}\mathbf{v}$$

where $\boldsymbol{\sigma}$ and $\mathbf{v}$ are the stress tensor and the velocity vector, respectively. It gives, by its modulus and direction, the power flow through a continuous medium and permits one to write the local power balance in the form

$$div\,\mathbf{I} + \Pi_{diss} = \partial e/\partial t \tag{1}$$

with Π_{diss} and $\partial e/\partial t$ being, respectively, the dissipated power and the time derivative of the total energy (kinetic and potential).

The transmission potential function has been introduced in reference [26, 29].

Here the Poynting vector field is represented by the sum of an irrotational and a solenoidal field using the Helmholtz–Clebsch decomposition,

$$\mathbf{I} = grad\,\psi + rot\,\boldsymbol{\Psi}, \tag{2}$$

where ψ and $\boldsymbol{\Psi}$ are the scalar and the vector potential respectively. By combining equation (2) and the power balance (1), one has

$$\nabla^2\psi + \Pi_{diss} = \partial e/\partial t. \tag{3}$$

Therefore, in the power balance only the scalar potential appears (namely, the transmission potential), being the power flow related only to the divergence of the Poynting vector. Obtaining an energy equation requires giving explicit expressions for ψ and Π_{diss} in terms of e. Therefore, the problem of providing the energy constitutive relationships consists of the following steps: determination of the correlation $\psi = \psi(e)$; and determination of the correlation $\Pi_{diss} = \Pi_{diss}(e)$.

To this end an appropriate energy definition must be established; the nature of the energy equation depends on this choice. In the framework of the conductivity principle, it is convenient to consider some energy average in time, frequency or space, so that the energy equation could be simpler than the original equation of motion, but still useful for the prediction of the structural response.

When harmonic motion and time average are considered, the following dissipation constitutive equation is definitely accepted [33]:

$$\Pi_{diss} = 2\eta\omega\langle e\rangle, \qquad \langle e\rangle = \frac{1}{2T}\int_{-T}^{T}\frac{1}{2}\rho\omega^2\dot{w}^2\,\mathrm{d}t.$$

Here η, ω and T are loss factor, the circular frequency and the period of oscillation respectively. This is a good and simple approximation of the dissipated power. As a consequence of this assumption the time derivatives of the energy in equations (1) and (3) disappear.

For this case, the form of the function $\psi(e)$ was investigated in reference [26] and the fundamental results, for harmonic force, can be summarized as follows: the potential of transmission depends on two different terms of which only one (the thermal contribution, t) is proportional to the local stored energy: $\psi = \psi_t + \psi_d = \alpha\langle\bar{e}\rangle + \psi_d$; the second term ψ_d (deviation, d) is not only dependent on the energy: rather its expression is a complex function of the local displacement. Moreover it is not negligible with respect to the first one.

The same result can be extended to the spectral-average energy for a random excitation [26].

An important confirmation of these results is found in reference [29], where the general inconsistency of the thermal analogy has also been proved following a different mathematical approach.

The conductivity principle consists in admitting that the mechanical energy along a structure, obeys the law

$$\nabla^2\tilde{e} - \beta\tilde{e} = 0,$$

where the tilde denotes some kind of average operation on the energy e, such as frequency, time, space or ensemble average, according to different authors [13–15, 24, 27, 28].

Several theoretical considerations, numerical simulations and, finally, some experimental results [34], induce one to think that the space average is closely related to the energy transmission. Therefore, in the present paper, besides the time average, the space-average effects are also investigated. The idea, formally developed in the rest of the paper, of studying the power flow transmission in the structure through regions of characteristic finite size d, arises. On the basis of the previous results concerning the time-average energy, a close relationship of ψ_d to the total power transmission is expected if d/λ is small. On the other hand, if $d/\lambda \gg 1$, a different energy rate condition would be approached. Under this last hypothesis, an asymptotic analysis is developed and the implications on the contribution of ψ_d are discussed.

The following spatial moving-average definition is therefore assumed:

$$\langle\bar{e}(x,y,z)\rangle = \frac{1}{d^3}\int_D \langle e(x_1,x_2,x_3)\rangle\,\mathrm{d}x_1\,\mathrm{d}x_2\,\mathrm{d}x_3$$

$$D = \{x - d/2 < x_1 < x + d/2,\ y - d/2 < x_2 < y + d/2,\ z - d/2 < x_3 < z + d/2\}.$$

Here x_1, x_2, x_3 are three auxiliary space co-ordinates employed to perform the space average over D, while x, y, z are the space co-ordinates of the centroid of the D region.

3. ASYMPTOTIC THERMAL EFFECTS IN ONE-DIMENSIONAL WAVEGUIDES

Consider a beam, with suitable restraints on the boundary, subjected to point harmonic loads. The farfield displacement solution for this vibrating beam is

$$\hat{w}(x,t) = w(x)\mathrm{e}^{\mathrm{j}\omega t} = (a_- \mathrm{e}^{\mathrm{j}kx} + a_+ \mathrm{e}^{-\mathrm{j}kx})\mathrm{e}^{\mathrm{j}\omega t},$$

$$k = k_B(1 - \mathrm{j}\eta/4) = \sqrt[4]{\rho A\omega^2/EI}(1 - \mathrm{j}\eta/4),$$

k being the complex wavenumber, a_-, a_+ the wave phasors and η, E, A, I, ρ, ω the loss factor, Young's modulus, cross-sectional area, moment of inertia, mass density and the circular frequency of oscillation respectively. This expression completely represents the beam motion in each region far enough from the boundary and the point forces. In fact, in this case, the near field can be neglected and when the wave phasors are determined in a suitable way, the given expression represents the general motion of the beam in each of the mentioned regions.

The time-average energy is $\langle e \rangle = \frac{1}{2}\rho A\omega^2 w^* w$, which, after some mathematics, can be written as

$$\langle e \rangle = \frac{1}{2}\rho A\omega^2 [a\mathrm{e}^{-k_B(\eta/2)x} + b\mathrm{e}^{k_B(\eta/2)x} + c\cos(2k_B x + \varphi)]$$

where $a = |a_+|^2$, $b = |a_-|^2$, $c = 2|a_+ a_-^*|$ and $\varphi = \angle(a_+ a_-^*)$. The space-average energy defined by

$$\langle \bar{e}(x) \rangle = \frac{1}{d}\int_{x-d/2}^{x+d/2} \langle e(x_1) \rangle \, \mathrm{d}x_1$$

provides, after several manipulations, the relationship

$$\langle \bar{e} \rangle = \kappa_e \left[\left(\frac{\mathrm{e}^{\pi\mu\eta} - 1}{\pi\mu\eta \mathrm{e}^{\pi\mu(\eta/2)}} \right) (a\mathrm{e}^{-k_B(\eta/2)x} + b\mathrm{e}^{k_B(\eta/2)x}) + c\left(\frac{\sin(2\pi\mu)}{2\pi\mu} \right) \cos(2k_B x + \varphi) \right]$$

$$= \langle \bar{e} \rangle_t + \langle \bar{e} \rangle_d, \qquad \kappa_e = \frac{1}{2}\rho A\omega^2, \tag{4}$$

where t and d indicate the thermal and the deviation component respectively and $\mu = d/\lambda$ is introduced. This expression gives some important insights into the power flow transmission. In fact, one can immediately observe the double energy contribution: the first,

$$\langle \bar{e} \rangle_t = \kappa_e \left[\left(\frac{\mathrm{e}^{\pi\mu\eta} - 1}{\pi\mu\eta \mathrm{e}^{\pi\mu(\eta/2)}} \right) (a\mathrm{e}^{-k_B(\eta/2)x} + b\mathrm{e}^{k_B(\eta/2)x}) \right],$$

smooth, is governed by exponential terms and is thermal; on the contrary, the second one $\langle \bar{e} \rangle_d$ is harmonically oscillating. From this point of view, the situation does not differ much from that obtained using only the time-average energy [25, 26]. The relevant difference is here related to the presence of the μ dependent factors in the energy expression. Those terms control, through μ, the relative amplitudes of the two energy contributions and their asymptotic properties (as $\mu \to \infty$ or $\mu \to 0$) reveal two different energy rate regions: the small and the large μ scales.

When the local energy value is accounted for, corresponding to $d \to 0$, no space average is performed. In this case, $\mu \to 0$ and from equation (4) it is apparent that both the factors involving μ in the energy expression tend to 1. Therefore, the thermal and non-thermal components are of the same order of magnitude. On the contrary, the opposite asymptotic limit, $\mu \to \infty$, definitely increases the amplitude of the thermal components, while the non-thermal one tends to vanish. Moreover, if $\mu = n/2$ (for an integer n), the amplitude of the non-thermal component is zero.

It can be concluded that the thermal conductivity has an asymptotic validity in the sense previously defined: i.e., $\lim_{\mu \to \infty} \langle \bar{e} \rangle = \langle \bar{e} \rangle^{\infty} = \langle \bar{e} \rangle_t$.

To point out this wavelength scale effect better, it is interesting to estimate the thermal and non-thermal transmission potentials. The local energy balance gives $\psi'' - 2\eta\omega\langle e \rangle = 0$.

Substituting the obtained space-average energy expression (4) in it, and integrating twice with respect to x, one has for the potential,

$$\psi = 2\eta\mu \int\int \langle \bar{e} \rangle \, \mathrm{d}x \, \mathrm{d}x + c_1 x + c_2 \;\Rightarrow\; \psi = \frac{8\omega}{k_B^2 \eta} \langle \bar{e} \rangle_t - \frac{\eta\omega}{2k_B^2} \langle \bar{e} \rangle_d = \psi_t + \psi_d,$$

where the two constants in the potential expression can be sent to zero [26]. It is easy to verify the two properties:

$$\psi_d(x, \mu) = 0 \begin{Bmatrix} \mu \to \infty. & \text{(asymptotic property)} \\ \mu = n/2, & n = 1, 2, 3, \ldots \end{Bmatrix}.$$

This result has an important physical meaning: the deviation of the potential of transmission with respect to the thermal term becomes negligible if the space-average energy is computed over a domain whose characteristic size d is significantly greater than the wavelength λ. Moreover, when d equals a multiple of $\lambda/2$, the potential ψ is still totally thermal. Therefore, it can be concluded that, for the beam, the time- and space-average asymptotic energy $\langle \bar{e} \rangle^{\infty}$ satisfies the conductivity vibration principle.

4. ASYMPTOTIC BOUNDS IN TWO-DIMENSIONAL WAVEGUIDES NON-THERMAL ENERGY COMPONENT

The plate energy distribution follows a different governing law. The beam is a one-dimensional waveguide: the waves can travel only along a fixed direction. If

point harmonic loads are accounted for and the near field is neglected, one can represent the plate vibration solution by superposition of an infinite number of plane waves travelling in any possible direction. In other words, the displacement phasor w can be expressed as an integral in the form:

$$w(r) = \int_0^{\pi} a_+(\theta)\mathrm{e}^{-\mathrm{j}\mathbf{k}(\theta)\mathbf{r}} + a_-(\theta)\mathrm{e}^{\mathrm{j}\mathbf{k}(\theta)\mathbf{r}}\,\mathrm{d}\theta,$$

where $\mathbf{k}(\theta) = k_B(1 - \mathrm{j}\eta/4)\mathbf{n}(\theta)$ is the complex wave vector, $\mathbf{n}(\theta)$ the unit vector associated with the θ direction of propagation and $\mathbf{r} \equiv \{x, y\}$ the position vector. This is representative of the plate motion in every region far enough from the boundary and the point loads. The expression obtained is useful for a direct comparison between the beam and plate energy distributions. In fact, by starting from this formulation it is possible to proceed in the same way as shown in section 3. The time-average energy density per unit area associated with the displacement field is

$$\langle e\rangle = \kappa_T \int_0^{\pi}\int_0^{\pi} (a_+(\theta_1)\mathrm{e}^{-\mathrm{j}\mathbf{k}(\theta_1)\mathbf{r}} + a_-(\theta_1)\mathrm{e}^{\mathrm{j}\mathbf{k}(\theta_1)\mathbf{r}})$$

$$\times (a_+^*(\theta_2)\mathrm{e}^{\mathrm{j}\mathbf{k}^*(\theta_2)\mathbf{r}} + a_-^*(\theta_2)\mathrm{e}^{-\mathrm{j}\mathbf{k}^*(\theta_2)\mathbf{r}})\,\mathrm{d}\theta_1\,\mathrm{d}\theta_2,\ \kappa_T = \tfrac{1}{2}\rho\omega^2 h.$$

Developing the integrand expression, one obtains the time-average energy as

$$\langle e\rangle = \kappa_T \sum_{i=1}^{4} \int_0^{\pi}\int_0^{\pi} A_i(\theta_1, \theta_2)\mathrm{e}^{\mathbf{v}_i(\theta_1,\theta_2)\mathbf{r}}\,\mathrm{d}\theta_1\,\mathrm{d}\theta_2$$

where $A_1 = a_+(\theta_1)a_+^*(\theta_2)$, $A_2 = a_+(\theta_1)a_-^*(\theta_2)$, $A_3 = a_-(\theta_1)a_+^*(\theta_2)$ and $A_4 = a_-(\theta_1)a_-^*(\theta_2)$ are the wave energy coefficients and

$$\mathbf{v}_1 = \mathrm{j}\,|\mathbf{k}^*(\theta_2) - \mathbf{k}(\theta_1)|, \quad \mathbf{v}_2 = -\mathrm{j}\,|\mathbf{k}^*(\theta_2) + \mathbf{k}(\theta_1)|,$$

$$\mathbf{v}_3 = \mathrm{j}\,|\mathbf{k}^*(\theta_2) + \mathbf{k}(\theta_1)|,\ \mathbf{v}_4 = \mathrm{j}\,|\mathbf{k}^*(\theta_2) - \mathbf{k}(\theta_1)|.$$

According with the definition given in section 2, the space average over the D domain is therefore

$$\langle \bar{e}\rangle = \kappa_T \sum_{i=1}^{4} \int_0^{\pi}\int_0^{\pi} \frac{A_i(\theta_1, \theta_2)}{d^2}\left[\int_D \mathrm{e}^{\mathbf{v}_i\boldsymbol{\rho}}\,\mathrm{d}S\right]\mathrm{d}\theta_1\,\mathrm{d}\theta_2$$

$$= \kappa_T \sum_{i=1}^{4} \int_0^{\pi}\int_0^{\pi} \frac{A_i(\theta_1, \theta_2)\bar{E}_i(\mathbf{r}, \theta_1, \theta_2)}{d^2}\,\mathrm{d}\theta_1\,\mathrm{d}\theta_2,$$

where $\boldsymbol{\rho} = \{x_1, x_2\}$ (spatial co-ordinates). The inner integral is evaluated in the following manner:

$$\bar{E}_i(\mathbf{r}, \theta_1, \theta_2) = \int_{x-d/2}^{x+d/2}\int_{y-d/2}^{y+d/2} \mathrm{e}^{\mathbf{v}_i\boldsymbol{\rho}}\,\mathrm{d}x_1\,\mathrm{d}x_2 = \frac{\mathrm{e}^{\mathbf{v}_i\mathbf{r}}}{v_{ix}v_{iy}} \cdot \frac{\mathrm{e}^{v_{ix}d} - 1}{\mathrm{e}^{v_{ix}d/2}} \cdot \frac{\mathrm{e}^{v_{iy}d} - 1}{\mathrm{e}^{v_{iy}d/2}}.$$

4.1. ENERGY FIELD DECOMPOSITION

In the previous expression of the energy field, two main contributions can be separated. In fact, it is easy to show that the following decomposition holds:

$$\langle \bar{e} \rangle = \kappa_T \sum_{i=1}^{4} \int_0^{\pi} \int_0^{\pi} \frac{A_i(\theta_1, \theta_2) \bar{E}_i(\mathbf{r}, \theta_1, \theta_2)}{d^2} [1 - \delta(\theta_1 - \theta_2)] \, \mathrm{d}\theta_1 \, \mathrm{d}\theta_2 + \kappa_T \sum_{i=1}^{4} \int_0^{\pi} \frac{A_i(\theta, \theta) \bar{E}_i(\mathbf{r}, \theta, \theta)}{d^2} \, \mathrm{d}\theta,$$

$$\langle \bar{e} \rangle = \langle \bar{e} \rangle_{iwe} + \langle \bar{e} \rangle_{cwe}.$$

Here, δ is Dirac's generalized function and the two energy components are called *interference wave energy* (*iwe*) and *coincident wave energy* (*cwe*) respectively. The first is related to incident waves propagating along different directions, while the second is due to waves propagating in the same given direction. The properties of both are investigated separately in the following two sections.

4.1.1. *Coincident wave energy*

The explicit form of the *cwe* is recovered by introducing the expression for $\mathbf{v}_i(\theta_1, \theta_2)$, given previously, when $\theta_1 = \theta_2 = \theta$. One then has $\mathbf{v}_1 = -k_B(\eta/2)\mathbf{n}$, $\mathbf{v}_2 = -2\mathrm{j}k_B\mathbf{n}$, $\mathbf{v}_4 = k_B(\eta/2)\mathbf{n}$ and $\mathbf{v}_3 = 2\mathrm{j}k_B\mathbf{n}$, where $\mathbf{n} = \{\cos\theta, \sin\theta\}$. Substituting in the *cwe* expression one obtains, after some mathematics,

$$\langle \bar{e} \rangle_{cwe,t} = \kappa_T \int_0^{\pi} \left(\frac{(\mathrm{e}^{\pi\mu\eta\sin\theta} - 1)(\mathrm{e}^{\pi\mu\eta\cos\theta} - 1)}{(\pi\mu\eta)^2 \sin 2\theta \, \mathrm{e}^{\pi\mu(\eta/2)(\sin\theta + \cos\theta)}} \right) \cdot (A_1 \mathrm{e}^{-k_B(\eta/2)\mathbf{nr}} + A_4 \mathrm{e}^{k_B(\eta/2)\mathbf{nr}}) \, \mathrm{d}\theta,$$

$$\langle \bar{e} \rangle_{cwe,d} = \kappa_T \int_0^{\pi} \left(\frac{\sin(2\pi\mu\cos\theta)\sin(2\pi\mu\sin\theta)}{(\pi\mu)^2 \sin 2\theta} \right) |A_2| \cos(2k_B\mathbf{nr} - \varphi),$$

$$\langle \bar{e} \rangle_{cwe} = \langle \bar{e} \rangle_{cwe,t} + \langle \bar{e} \rangle_{cwe,d},$$

Here $\varphi = \angle A_2$. The analogy between this part of the plate energy and the beam energy is complete. In fact, the first term is thermal and satisfies the conductivity law. On the contrary, the second one is non-thermal but has the same asymptotic properties discussed in section 3 about the beam energy. Therefore, the $\langle \bar{e} \rangle_{cwe}$ provide a substantial thermal energy contribution. Proceeding in the same manner as in section 3, when high μ values are considered (i.e., $\langle \bar{e} \rangle_{cwe,d}$ vanishes), the asymptotic *cwe* energy obeys the thermal law, i.e., $\nabla^2 \langle \bar{e} \rangle_{cwe}^{\infty} - (\eta\omega/c_g)^2 \langle \bar{e} \rangle_{cwe}^{\infty} = 0$, where c_g is the group velocity of flexural waves. The asymptotic transmission potential is therefore $\psi_{cwe}^{\infty} = (2\omega/c_g k_B)^2 \langle \bar{e} \rangle_{cwe}^{\infty}$.

It is important to notice that the possibility of spliting the *cwe* energy into two independent components is related to the form of the $\mathbf{v}_i$ vectors. They are two real ($i = 1, 4$) and two purely imaginary ($i = 2, 3$) component. Consequently two exponentially decaying and two harmonically oscillating (but asymptotically vanishing) solutions are found.

4.1.2. *Interference wave energy*

One can now examine the part of the energy related to the waves' interference. It is convenient to introduce the notations $\bar{E}_i(\mathbf{r}, \theta_1, \theta_2)/d^2 = F_i(\theta_1, \theta_2)\mathrm{e}^{\mathbf{v}_i \mathbf{r}}$, $\mathbf{v}_i(\theta_1, \theta_2) = k_B \mathbf{z}_i(\theta_1, \theta_2)$, where

$$\mathbf{z}_1 = -(\eta/4)(\mathbf{n}(\theta_1) + \mathbf{n}(\theta_2)) - \mathrm{j}(\mathbf{n}(\theta_1) - \mathbf{n}(\theta_2)),$$

$$\mathbf{z}_2 = (\eta/4)(\mathbf{n}(\theta_2) - \mathbf{n}(\theta_1)) - \mathrm{j}(\mathbf{n}(\theta_1) - \mathbf{n}(\theta_2)),$$

$$\mathbf{z}_3 = -\mathbf{z}_2, \qquad \mathbf{z}_4 = -\mathbf{z}_1.$$

The expression for $\langle \bar{e} \rangle_{iwe}$ is then

$$\langle \bar{e} \rangle_{iwe} = \kappa_T \sum_{i=1}^{4} \int_0^{\pi} \int_0^{\pi} \{A_i(\theta_1, \theta_2) F_i(\theta_1, \theta_2) \mathrm{e}^{\mathbf{v}_i \mathbf{r}} [1 - \delta(\theta_1 - \theta_2)]\} \, \mathrm{d}\theta_1 \, \mathrm{d}\theta_2 .$$

The $\mathbf{v}_i$, $\mathbf{z}_i$ vectors are generally complex and, thus, the integrand contains both evanescent and harmonic coupled factors. After mathematical manipulations, the following expression is obtained:

$$\langle \bar{e} \rangle_{iwe} = \kappa_T \sum_{i=1}^{4} \int_0^{\pi} \int_0^{\pi} \{A_i(\theta_1, \theta_2)(F_i^R(\mu, \theta_1, \theta_2) \cos(\mathbf{v}_i^I \mathbf{r}) - F_i^I(\mu, \theta_1, \theta_2) \sin(\mathbf{v}_i^I \mathbf{r})) \mathrm{e}^{\mathbf{v}_i^R \mathbf{r}} [1 - \delta(\theta_1 - \theta_2)]\} \, \mathrm{d}\theta_1 \, \mathrm{d}\theta_2 .$$

Here the symbols R and I indicate real and imaginary parts respectively, and the dependence on μ is explicitly indicated. This energy does not satisfy the thermal equation, as can be proved by direct substitution. Therefore, it is worthwhile to analyze the trend of the function F_i versus μ to evaluate the asymptotic effect of the interference components. The explicit form of F_i is

$$F_i(\mu, \theta_1, \theta_2) = \frac{(\mathrm{e}^{2\pi\mu z_{ix}^R} \mathrm{e}^{2\pi \mathrm{j} \mu z_{ix}^I} - 1)(\mathrm{e}^{2\pi\mu z_{iy}^R} \mathrm{e}^{2\pi \mathrm{j} \mu z_{iy}^I} - 1)}{(2\pi\mu)^2 z_{ix} z_{iy} \mathrm{e}^{\pi\mu z_{ix}^R} \mathrm{e}^{\pi\mu z_{iy}^R} \mathrm{e}^{\pi \mathrm{j} \mu z_{ix}^I} \mathrm{e}^{\pi \mathrm{j} \mu z_{iy}^I}} .$$

The exponents affecting the asymptotic trend of this function are only the real ones. Therefore, the asymptotic analysis of F_i involves the general function $\mathrm{e}^{2\alpha\mu}/\mu\mathrm{e}^{\alpha\mu}$, with the asymptotic property

$$\lim_{\mu \to \infty} \frac{\mathrm{e}^{2\alpha\mu}}{\mu \mathrm{e}^{\alpha\mu}} = \begin{cases} 0 & \text{if } \alpha < 0, \\ \infty & \text{if } \alpha > 0. \end{cases}$$

Since α is the real or imaginary part of the generic $\mathbf{z}_i$ vector, when θ_1, θ_2 vary in the integration region $\Theta \equiv [0; \pi] \times [0; \pi]$ α belongs to the interval $-\eta/2 < \alpha < \eta/2$. Therefore, in the part of Θ in which $\alpha < 0$, F_i tends to zero when μ increases, but in the remaining part of Θ it tends to infinity. Looking at the $\mathbf{z}_i$ vector expressions, one is easily convinced that for each region $\Re_- \subseteq \Theta$ over which $\alpha < 0$ there exists a corresponding $\Re_+ \subseteq \Theta$, of equal area, over which $\alpha > 0$. Consequently, the integrand of the *interference wave energy* has globally the same exponential increasing trend as the contributions in the integral of the *coincident wave energy*. Thus, a non-thermal component definitely exists, even when the

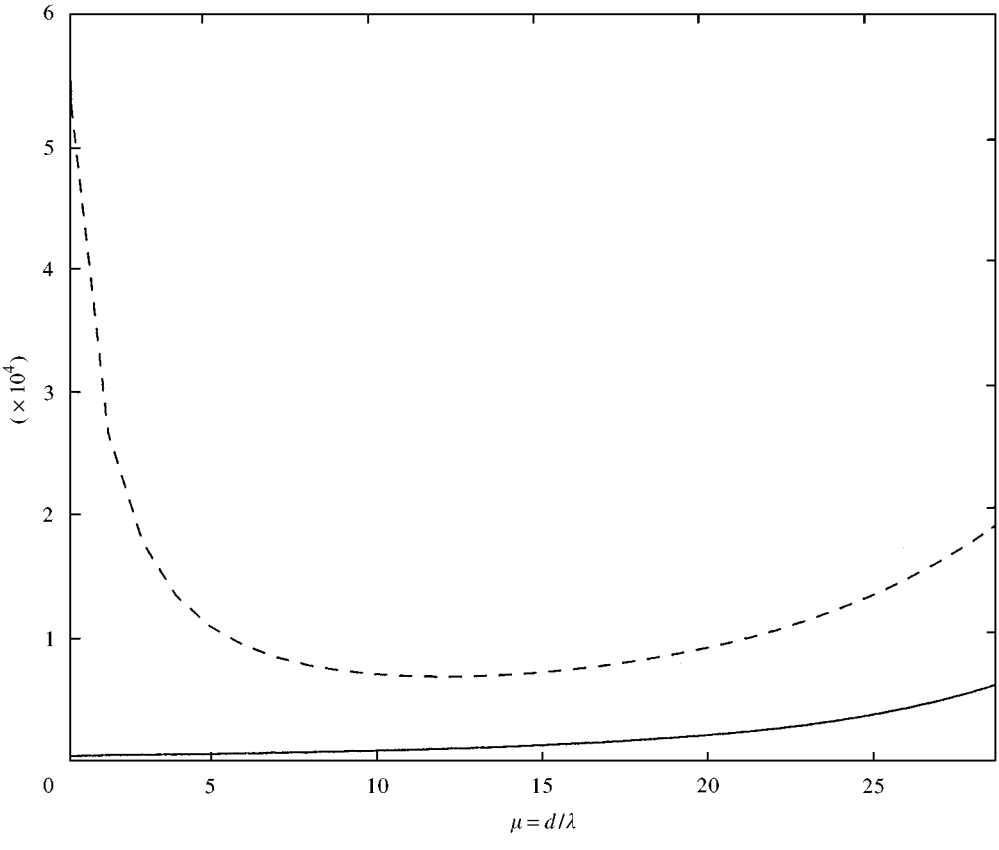

Figure 1. Comparison between non-thermal energy (---) and thermal energy (—), versus the scale range parameter μ.

asymptotics we considered. It should also be noticed that the combined effect of an increasing and a decreasing component of *iwe* can determine a relative minimum in its contribution to the total energy (see the later Figure 1).

Therefore, $\langle \bar{e} \rangle_{iwe}$ is generally not negligible with respect to $\langle \bar{e} \rangle_{cwe}$. The complete energy field consists of the thermal (t) and deviation (d) components of *cwe* and of the *iwe* contribution: i.e.,

$$\langle \bar{e} \rangle = \langle \bar{e} \rangle_{cwe,t} + \langle \bar{e} \rangle_{cwe,d} + \langle \bar{e} \rangle_{iwe}$$

with the asymptotic property

$$\lim_{\mu \to \infty} \langle \bar{e} \rangle = \langle \bar{e} \rangle_{cwe}^{\infty} + \langle \bar{e} \rangle_{iwe}^{\infty},$$

where $\langle \bar{e} \rangle_{iwe}^{\infty}$ does not satisfy the thermal law. In addition, it is important to point out that neither $\langle \bar{e} \rangle_{cwe,d}$ nor $\langle \bar{e} \rangle_{iwe}$ has any zero value in correspondence to multiples of the wavelength, as in the one-dimensional case.

One is easily convinced that a parallel analysis, leading to analogous results, can be developed for three-dimensional structures.

4.2. SOME REMARKS ABOUT THE WAVE ENERGY COEFFICIENTS

Before concluding this part of the analysis, further considerations about the energy coefficients $A_i(\theta_1, \theta_2)$ must be added. It is difficult to make any general prediction about their form, since they are very sensitive to the plate geometry and to the force location. However, two opposite extreme conditions can be analyzed as follows.

In recent paper [25], an average of them is proposed (spatial, ensemble, etc.) by introducing an expected value operator E. Even if the present paper is mainly devoted to the moving-space average, introduced by μ, the question deserves particular attention especially in evaluating the damping effects. The accepted hypothesis in reference [25] is substantially, $E[A_i(\theta_1, \theta_2)] = A_i \delta(\theta_1 - \theta_2)$. The main consequence of this assumption is that only the coherent energy terms $(\theta_1 = \theta_2)$ are preserved by the action of the E operator and they constructively take part only in the total energy field. This condition is called here *statistical directional independence* (*sdi*).

In the frame of the present analysis this means that the energy amplitude coefficients of the *interference wave energy* produce, on average, a zero contribution, or a negligible contribution with respect to the *coincident wave energy* coefficients. Therefore, the thermal component would be prevalent with respect to the non-thermal one.

However this assumption, as shown in reference [25], is incorrect in axisymmetric problems. It is important to point out that in these cases the energy distribution does not depend at all on the propagation angle θ, and this is in apparent contradiction with the *sdi* assumption. In fact, important corrections to the thermal analogy are proposed in reference [25] for analysis of this kind of problem.

In the present paper, point loads on the structure are being analyzed. The action of the force generates circular waves propagating from the force location towards the boundaries of the structure. When these circular train waves (direct field) reach the boundaries, the reflections generate a reverberant field. Thus, when dealing with point forces, the direct field is always axi-symmetric which violates the *sdi* hypothesis. This happens irrespectively of the nature of the point force, be it harmonic or random. Moreover, as discussed in the next section, this effect is amplified when high damping is involved.

Therefore, when approaching axisymmetric propagation, the energy coefficients rather obey the *isotropic condition* (*ic*) $E[A_i(\theta_1, \theta_2)] = A_i$. However, even for low damping and even admitting that the reverberant field could obey the *sdi* hypothesis, the direct field, in the point load case, is always axisymmetric and obeys the isotropic condition. Thus, at least for the point force case (harmonic and random in time), the *sdi* hypothesis fails.

The energy behaviour when the *ic* hypothesis is accepted is now analyzed.

Assume, for the sake of simplicity, the *ic* in the form $A_i = 1$. In this case, both the energy components $\langle \bar{e} \rangle_{iwe}$ and $\langle \bar{e} \rangle_{cwe}$ can be numerically evaluated using the general formulas found in the previous two sections. Their trend versus μ is plotted in Figure 1. The importance of the non-thermal energy contribution and even its

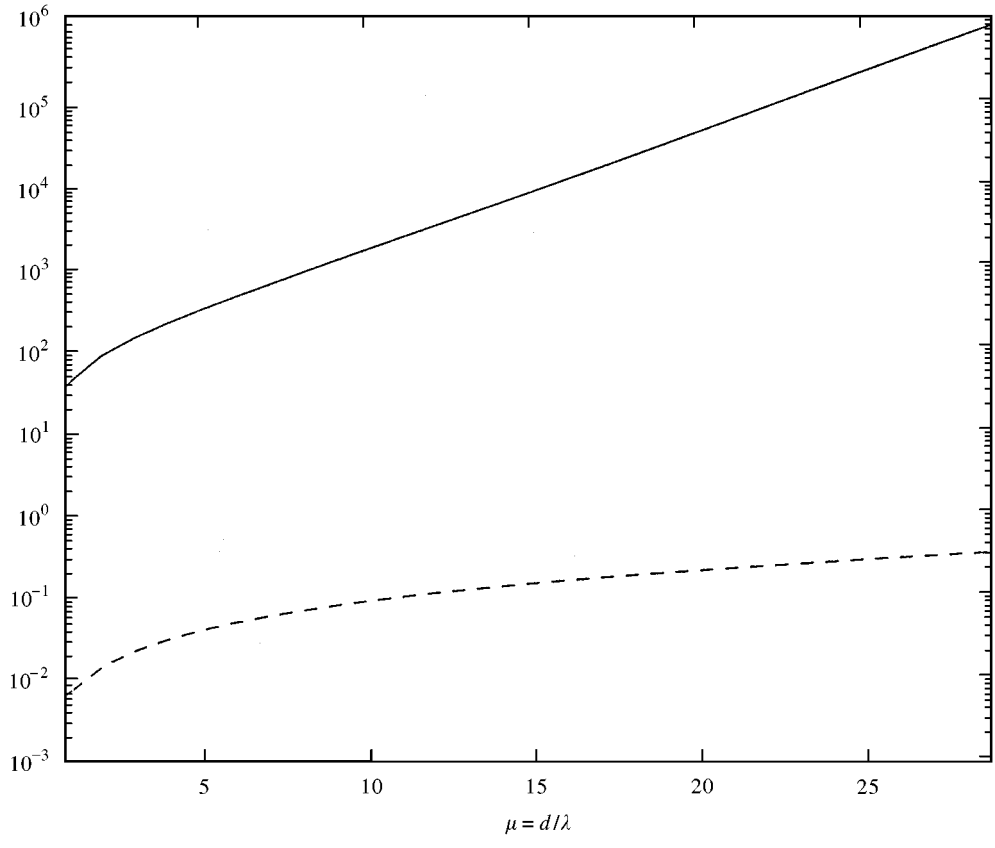

Figure 2. Thermal/non-thermal energy ratio versus μ: different behaviour between (—) beam and plate (---).

strong prevalence over the thermal one are appearent. Moreover, the previously quoted $\langle \bar{e} \rangle_{iwe}$ minimum appears.

In Figure 2, a comparison between the beam and the plate energy is shown. More precisely, the thermal to non-thermal energy ratio is plotted versus μ, when for the plate the *ic* hypothesis is used, confirming the difference between the one- and two-dimensional laws of energy distribution.

These results are rather interesting. In fact, one can suppose that the form of the wave energy coefficients $A_i(\theta_1, \theta_2)$ generally has behaviour intermediate between the two *sdi* and *ic* cases. As a consequence, the non-thermal energy contribution generally belongs, with reference to Figure 1, to the region bounded by the μ-axis (zero *iwe* contribution accordingly with the *sdi* hypothesis) and the dashed curve (*ic* hypothesis).

5. ON THE ROLE OF DAMPING IN THE THERMAL ANALOGY

In the previous section, the importance of μ has been discussed for one- and two-dimensional systems.

The damping effects on the mechanism of wave energy propagation now deserves particular attention. In fact, dissipation phenomena imply very different effects when considering one- or two-dimensional systems. Moreover, their role is crucial for the validity of the thermal conductivity approach.

5.1. ONE-DIMENSIONAL SYSTEMS

If in the thermal balance the dissipation is not considered, i.e., the loss factor is zero, the balance equation collapses into a Laplace equation. In this case, when adiabatic boundary conditions are imposed, the problem encounters serious difficulties. In fact, the input power must be zero because the total dissipated energy is zero (global power balance of the structure) and, consequently, the forcing term in the thermal equation is also zero. For a one-dimensional system

$$\langle \bar{e} \rangle'' = 0 \text{ along the guide}, \qquad \langle \bar{e} \rangle' = 0 \text{ on the boundaries}$$

so that one has

$$\langle \bar{e} \rangle = ax + b, \qquad \langle \bar{e} \rangle' |_0^t = 0 \Rightarrow \langle \bar{e} \rangle = b.$$

Therefore, a constant value of the average energy level on the beam is found. In addition, its value is unknown because no physical information provides it. Moreover, this solution is wrong, at least for harmonic point load. In fact, for the undamped beam, subject to a point force, sudden jumps in the average energy appear [35]. Similar conclusions hold when a small damping factor η is considered. In this case, the average energy level is recovered trivially by the power balance

$$2\eta\omega \int_D \langle e \rangle \, \mathrm{d}x = P_{in} \rightarrow 2\eta\omega L \left\{ \frac{1}{L} \int_0^L \langle e \rangle \, \mathrm{d}x \right\} = P_{in} \rightarrow \langle e \rangle \approx \frac{P_{in}}{2\eta\omega L},$$

where L is the beam length and P_{in} the injected power. This equation provides, more simply, the same solution as obtained by the thermal conductivity approach, requiring the same *a priori* information, i.e., P_{in}.

On the other hand, if a heavy damping effect is considered, the thermal analogy is asymptotically successful (in the sense specified in section 5.1). In fact, in the energy expression (4) the non-thermal component is independent of η, but the thermal one depends on it by the factor $(\mathrm{e}^{\pi\mu\eta} - 1)/\pi\mu\eta\mathrm{e}^{\pi\mu\eta/2}$. The ratio between the thermal and non-thermal energy amplitudes when η increases is

$$\lim_{\eta \to \infty} \frac{\mathrm{e}^{\pi\mu\eta} - 1}{\pi\mu\eta\mathrm{e}^{\pi\mu\eta/2}} = \mathrm{e}^{\pi\mu\eta}.$$

It can be concluded that larger the η, greater the thermal energy component with respect to the non-thermal one. In this case, even for a point load harmonic force, the jump effect at the force location tends to disappear [35] and the energy trend prediction is accurate.

5.2. TWO-DIMENSIONAL SYSTEMS

In this case, when the damping factor approaches zero, again some difficulties arise. In fact, one has

$$\nabla^2 \langle \bar{e} \rangle = 0 \text{ along the structure,} \qquad \partial \langle \bar{e} \rangle / \partial n = 0 \text{ on the boundary.}$$

A simple property of elliptic differential equations [36] states that if the harmonic function $\langle \bar{e} \rangle$ has normal derivatives vanishing on the boundary ∂D, then the function is constant on D. Thus, when a lightly damped structure is considered in the frame of the thermal analogy, an almost constant energy distribution is expected. Its average (representative of the energy distribution) is simply obtained by

$$2\eta\omega \int_D \langle \bar{e} \rangle \, \mathrm{d}S = P_{in} \to 2\eta\omega S \left\{ \frac{1}{S} \int_D \langle \bar{e} \rangle \, \mathrm{d}S \right\} = P_{in} \to \langle \bar{e} \rangle \approx \frac{P_{in}}{2\eta\omega S}.$$

Therefore, even in the two-dimensional case, for small η, the thermal conductivity is of little practical importance.

The analysis of heavily damped structures is more complicated. In the previous section, the energy field decomposition $\langle \bar{e} \rangle = \langle \bar{e} \rangle_{cwe,t} + \langle \bar{e} \rangle_{cwe,d} + \langle \bar{e} \rangle_{iwe}$ was suggested. The first two terms are the one-dimensional-like energy components. Therefore, when the damping factor increases, the $\langle \bar{e} \rangle_{cwe,t} / \langle \bar{e} \rangle_{cwe,d}$ ratio definitely increases, approaching a thermal behaviour (section 5.1)

A second effect is related to the expression of F_i given in section 4.1.2. One is easily convinced that when η is increased, in the asymptotic limit $\mu \to \infty$, F_i and thus *iwe*, is also increased. Therefore, under this respect, an increasing of η leads to increase *iwe*.

A third opposite effect is instead observed for the interference energy component. In fact, when heavy damping is considered, the energy direct field rapidly decreases from the power injection point. Then the amount of energy that reaches the boundary to initiate the reverberant field is small compared with that of the direct field, thus eluding the *sdi* assumption. In such a case, an axisymmetric distribution is approached and the thermal analogy fails.

However, the two first opposite effects examined do not tend to a compensation. When assuming the *ic* hypothesis, the thermal to non-thermal energy ratio is plotted versus μ for different values of the damping factor in Figure 3. The increasing importance of the non-thermal component as the damping factor increases is apparent.

From the previous considerations the following conclusions about the dissipation effect on the energy transmission mechanism, can be drawn.

For a low damping factor: (i) the thermal analogy predicts an almost constant energy distribution, and in this case its utility is doubtful because the energy level is substantially proportional to the input power and immediately computed; (ii) in general, when a point harmonic force is considered, the constant energy level prediction is incorrect; in fact in corresponding to the force location, a sudden jump in the energy level appears (in both one- and two-dimensional systems).

For a high damping factor: (i) for one-dimensional systems, a high dissipation leads fast to an asymptotic thermal transmission (as specified in section 3); the

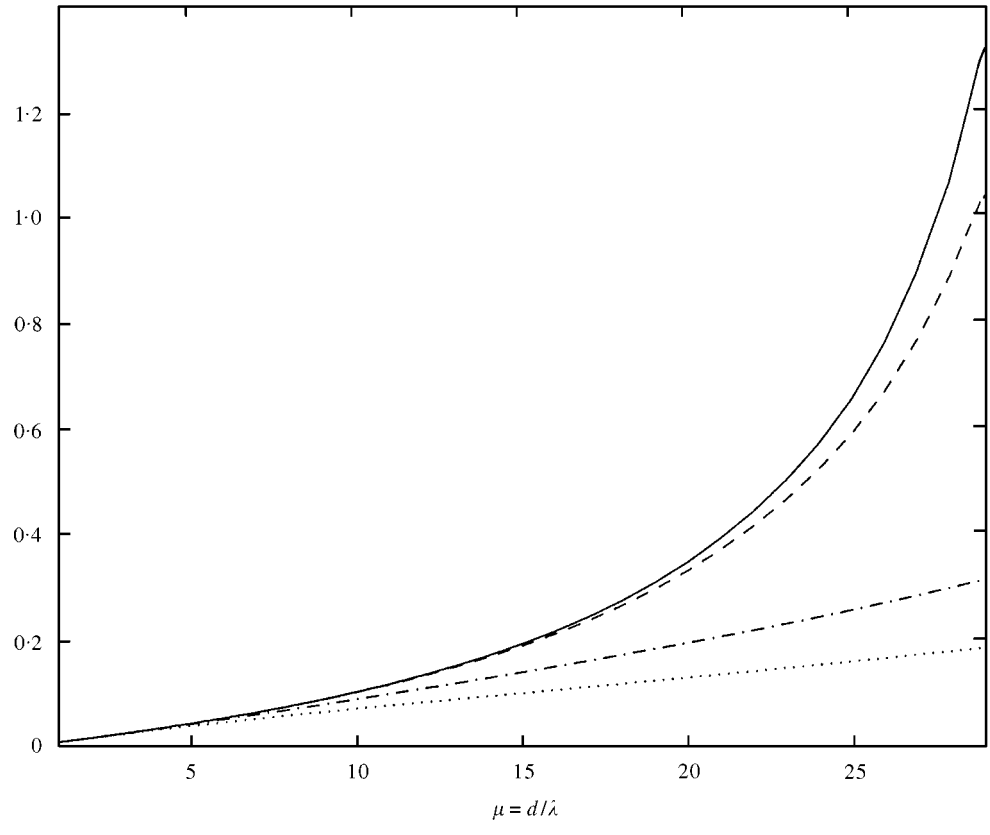

Figure 3. Thermal/non-thermal energy ratio versus μ, when varying the damping factor η. η onlines: ——, 0·001; – – –, 0·01, – · – · –, 0·05, ·····, 0.1.

sudden energy jump at the force location tends to disappear and the thermal prediction is correct; (iii) for two-dimensional systems the dissipation effect acts an opposite manner on the two main energy components: η speeds up the one-dimensional-like energy contribution $(\langle \bar{e} \rangle_{cwe,t} + \langle \bar{e} \rangle_{cwe,d})$ convergence towards the asymptotic thermal distribution (when μ is large enough); on the contrary, the non-thermal interference component increases its importance with respect to the thermal one.

6. EXPERIMENTAL VALIDATION OF THE THEORY

In the first part of this paper, the basic principle of thermal propagation of mechanical energy has been examined from a theoretical point of view. The results suggest that the analogy between thermal and mechanical energy propagation would be an acceptable approximation only for one-dimensional systems, but is no longer valid in general for two- and three-dimensional structures.

An experimental validation of the theoretical predictions is now presented.

The experimental tests were performed on a beam and a plate, excited in a relatively high-frequency range. Consequently, short characteristic wavelengths are generated and a very fine measurement grid is required. A measurement technique, based on a scanner laser vibrometer is, in this case, the most effective way to investigate the phenomenon. The comparison between theory and experimental results confirms the dependence of the energy transmission law on the wavelength scale effect and outlines a different energy rate law for beams and plates.

Although conceptually not difficult, the experimental analysis requires some preliminary discussion about two main points.

The first is related to the variations of μ needed to investigate the asymptotic properties of the power flow. In fact, a systematic set of tests must be performed at different values of μ.

Since μ is defined as $\mu = d/\lambda = dk_B/2\pi = d\omega/2\pi c_B$, it is evident that the variations of μ can be obtained in two totally different ways: acting on the circular frequency or on the cell size d.

In this way, doubt that the effects produced on the energy transmission mechanism can be different arises. This, in fact, is what was observed in several computer simulations used to design the experimental work. However, it must now be noticed that the theoretical analysis implicitly assumes that one varies d and not λ. In fact, in the space-average energy expression [e.g., equation (4), or plate energy expressions given in section 4] both μ and $k_B = 2\pi/\lambda$ appear. But the asymptotic analysis accounts only for μ variations, while k_B (i.e., λ) has been assumed to be constant. Therefore, experimental and theoretical results must be compared under the same hypothesis: i.e., by varying μ acting only on d. However, a suitable dimensional analysis, developed in section 6.1, helps in a further understanding of the problem.

The second concerns the experimental analysis of the thermal and non-thermal energy components that cannot be individually measured. Therefore, an indirect evaluation of them is required. In section 6.2, a simple approach to this problem is proposed. The idea consists in measuring the total energy field along the structure. Then, by using the thermal assumption, the power balance of each subregion can be written in thermal form but since the total energy does not generally obey this law, an equation error arises and it is assumed as a measure of the deviation component of the energy flow with respect to the power rate predicted by the thermal hypothesis.

6.1. DIMENSIONAL ANALYSIS OF THE POWER EXCHANGE

Consider a partition of the structure into elements of characteristic size d. The relevant physical properties of each cell are related to E, ρ, η and v (Poisson's ratio); the cell geometry is then completely described by its thickness h and its characteristic size d. The information about the time evolution of the physical quantities is given by the circular frequency ω.

E, ρ, η, v, h, d, ω can be assumed as the seven physical relevant quantities governing the energy exchange between two contiguous cells.

The following relationships hold:

$$\lambda = 2\pi/\sqrt[4]{\rho h\omega^2/D}, \qquad D = Eh^3/12(1-\nu^2), \qquad c_L = \sqrt{E/\rho},$$

and it is convenient to replace h, ν, E by λ, D, c_L respectively. Since mechanical energy propagation is considered, the fundamental physical quantities to account for are: length (L), mass (M) and time (T). The Buckingham Π theorem states that the number of basic non-dimensional groups is given by the difference between the number of independent characteristic quantities (seven) and the fundamental ones (three): i.e., four non-dimensional groups can be recovered ($\Pi_1, \Pi_2, \Pi_3, \Pi_4$). Consider, for example, the power flow: it must depend on four non-dimensional groups. Their form is easily determined by the Buckingham method:

$$\Pi = \Pi_1\Pi_2\Pi_3\Pi_4 = d^\alpha \lambda^\beta c_L^\gamma \rho^\delta \eta^\varepsilon D^\zeta \omega^\xi,$$

Π being a non-dimensional quantity. By introducing explicitly L, M, T into the previous expression and solving the dimensional equation in terms of the unknown exponents, one obtain

$$\Pi = \left(\frac{d}{\lambda}\right)^\alpha \left(\frac{c_L}{\omega\lambda}\right)^\gamma \left(\frac{D}{\omega^2\lambda^5\rho}\right)^\zeta \eta^\varepsilon.$$

These are the four characteristic non-dimensional groups sufficient to describe the energy transmission between the subsystems in which the structure is partitioned. It must be noticed that the first is just the μ parameter: it depends only on the cell size d. The physical consequence is remarkable. When interested in studying the dependence of the energy transmission on the μ parameter, one must act on the cell size d only. If the wavelength λ is modified, acting on the frequency, then three non-dimensional groups are modified. These considerations suggest performing set of experimental measurements at constant frequency by varying the cell size over which the energy average is computed.

The damping factor has also, as expected, an important role in the energy transfer. The implications for the thermal analogy of the dissipation effect has been analyzed previously in this paper.

Here attention is mainly addressed to the μ factor because it involves d, i.e., it is directly related to the definition of the moving-average energy introduced in the first part of the paper. In other words, once the wavelength is given, one is able to modify μ without involving any modification (geometrical or in the physical parameters) in the system analyzed.

6.2. INDIRECT MEASURE OF THE NON-THERMAL FLOW

In section 4, the analysis of the power flow was carried out by introducing the energy components of the whole energy field. The asymptotic behaviour of each component was discussed and their properties described. This way of analyzing the energy constitutive relationships is suitable when approaching the problem theoretically. On the contrary, when dealing with experimental tests, it is possible

only to measure the whole energy field and no direct information on single energy components is available. The solution of this problem relies on an indirect inspection of these contributions by measuring some of their observable effects. Here the calculation of the non-thermal energy flow is proposed, through the indirect estimate of the equation error as described in what follows.

First consider the kinetic energy related to the beam motion. The theoretical considerations developed in section 3 allow one to state that only the $\langle \bar{e} \rangle_t$ energy component is thermal, i.e., satisfies the governing equation

$$\frac{8\omega}{k_B^2 \eta} \langle \bar{e} \rangle_t'' - 2\eta\omega \langle \bar{e} \rangle_t = 0.$$

Therefore, the complete energy field $\langle \bar{e} \rangle$ generally does not obey the heat law and when substituting $\langle \bar{e} \rangle$ in the thermal equation, a local flow error ε_x is introduced:

$$(8\omega/k_B^2 \eta) \langle \bar{e} \rangle'' - 2\eta\omega \langle \bar{e} \rangle = \varepsilon_x. \tag{5}$$

Making use of the energy expression (4), one has (if $\eta \ll 1$)

$$\varepsilon_x(x, \mu) \approx 8k_B^2 \kappa_e \eta\omega c \frac{\sin 2\pi\mu}{2\pi\mu} \cos(2k_B x + \varphi). \tag{6}$$

A global flow error can be also introduced by integrating ε_x^2 over the beam's length, i.e.,

$$\varepsilon(\mu) = \sqrt{\frac{1}{l} \int_0^l \varepsilon_x^2(x, \mu)\, \mathrm{d}x} \approx 4\sqrt{2} k_B^2 \kappa_e \eta\omega c \frac{\sin 2\pi\mu}{2\pi\mu}.$$

It is apparent that the equation error tends to zero as μ increases and is zero when $\mu = n/2$, with an integer n. These results are exactly the same obtained in section 3, although expressed in an alternative form, more convenient in an experimental validation of the theory. Therefore, ε can be used as a check parameter of the power flow deviation, with respect to that predicted by the thermal assumption.

The flow error and related asymptotics can be also introduced in a slightly different manner. Consider the beam, decomposed into N segments of length d, as a set of physical subsystems connected in series. The time-average energy, per unit length, stored in the ith system is $\bar{E}_i = \langle \bar{e}(x_i) \rangle$, where x_i is the centre of the segment considered and $\langle \bar{e}(x_i) \rangle$ is given by equation (4).

When a proportional energy transmission law is assumed, the power flow Φ, the dissipated power Π_{diss}, related to the ith segment and the transmitted power $\Pi_{tr,i}$, between the ith and the $(i+1)$-th segments, are, respectively,

$$\Pi_{tr,i} = -f \frac{(\bar{E}_{i+1} - \bar{E}_i)}{d} \quad \Phi_i = -(\Pi_{tr,i} - \Pi_{tr,i-1}) = f \frac{(\bar{E}_{i+1} - 2\bar{E}_i + \bar{E}_{i+1})}{d},$$

$$\Pi_{diss,i} = 2\eta\omega \bar{E}_i d.$$

Thus, the power balance of the ith segment is

$$\Phi_i - \Pi_{diss,i} = \varepsilon_i, \qquad f\,\frac{(\bar{E}_{i+1} - 2\bar{E}_i + \bar{E}_{i+1})}{d^2} - 2\eta\omega\bar{E}_i = \varepsilon_i, \tag{7}$$

where f is a proportionality constant, whose value can be determined using the procedure shown in the next section. Equation (7) represents, in some way, the finite counterpart of equation (5) and is suitable for the experimental measure of the flow error. An explicit expression of the flow error can be found in Appendix A.

$$\varepsilon_i = 2\eta\omega\left[\frac{2(\cos 4\pi\mu - 1)}{(\pi\mu\eta)^2} - 1\right]\kappa_e c\,\frac{\sin 2\pi\mu}{2\pi\mu}\cos(2k_B x_i + \varphi), \tag{8}$$

showing that the asymptotic properties of ε_i are qualitatively similar to those discussed in equation (6). A dimensionless global error can also be defined as

$$\varepsilon = \sqrt{(1/N)\sum_{i=1}^{N}\varepsilon_i^2}/(\textstyle\sum_{i=1}^{N}\Pi_{diss,i}) = \sqrt{(1/N)\sum_{i=1}^{N}\varepsilon_i^2}/\Pi_{diss}\,.$$

The previous remarks about the power flow error indicate that ε is a measure of the total amount of non-thermal power flow, i.e., it is the normalized power flow transmitted by the non-thermal energy component, and that the analysis of the trend of ε versus μ allowing to investigate the asymptotic properties of the non-thermal energy, as shown by equation (6), so the theory can be validated investigating the function $\varepsilon(\mu)$.

Moreover, the theoretical power analysis developed in the previous part of the paper, applies in two different ways. In fact, it is possible to check if the energy variable $\langle\bar{e}(x)\rangle$, considered a moving-space average, satisfies the thermal differential equation (4). On the other hand, $\bar{E}_i = \langle\bar{e}(x_i)\rangle$ provides the energy stored in a region of centre x_i and characteristic size d. Therefore, it is meaningful to study whether the energy exchange between bordering regions, considered as individual physical subsystems, follows or not the proportional thermal energy propagation, leading to the difference equation (7). The two different points of view lead, however, to rather similar conclusion about the asymptotic trend of the non-thermal flow, as is clearly shown by comparing equation (6) with equation (8).

With these considerations in mind, a detailed analysis of the power flow error is developed in the following as an indicator of the tendency of the energy to violate the thermal law.

A detailed analysis of the flow error criterion for the plate test case is as follows.

By laser measurements, the velocity phasor $W_{i,j}$, in each point $P_{i,j}$ of the grid is available. Therefore, once the energy density distribution over the grid is determined as $\langle e\rangle_{i,j} = \kappa_T W_{i,j}^* W_{i,j}$, the structure is divided into rectangular regions of characteristic sizes $d_x d_y$. This operation generates a grid on the structure. Each cell of the grid is indicated by $C_{r,s}$. The energy average can be computed for each cell in the form

$$\langle\bar{e}\rangle_{r,s} = \frac{1}{d_x d_y}\sum_{i,j}^{n}\langle e\rangle_{i,j} = \frac{1}{d_x d_y}\sum_{i,j}^{n}\langle e(P_{i,j})\rangle, \quad \text{where } P_{i,j}\in C_{r,s},$$

$$C_{r,s} \equiv \{P : x_r - d_x/2 < x < x_r + d_x/2,\, y_s - d_y/2 < y < y_s + d_y/2\}. \tag{9}$$

At a fixed frequency ω a corresponding wavelength λ exists. Therefore, for each decomposition of characteristic sizes d_x, d_y (almost equal in the experimental case), a corresponding value of the μ parameter is determined, for example, as $\mu = d/\lambda = \sqrt{d_x d_y}/\lambda$. By varying the characteristic dimension of the cells, at a fixed frequency (see section 7.1), the desired μ parameter variations are obtained and, correspondingly, several distributions of the related average energy $\langle \bar{e}(\mu) \rangle_{r,s}$ are computed using equation (9).

The transmitted thermal powers, along x and y, are

$$\Pi^{(x)}_{tr,r} = -f \frac{\langle \bar{e} \rangle_{r+1,s} - \langle \bar{e} \rangle_{r,s}}{d_x} d_y, \qquad \Pi^{(y)}_{tr,s} = -f \frac{\langle \bar{e} \rangle_{r,s+1} - \langle \bar{e} \rangle_{r,s}}{d_y} d_x,$$

and therefore the thermal power balance of the rth, sth cell $C_{r,s}$ leads to

$$\Phi(\mu)_{r,s} - 2\eta\omega \langle \bar{e}(\mu) \rangle_{r,s} d_x d_y = \varepsilon(\mu)_{r,s}.$$

By developing the power flow expression it follows that

$$\Phi(\mu)_{r,s} = -(\Pi^{(x)}_{tr,r} - \Pi^{(x)}_{tr,r-1}) - (\Pi^{(y)}_{tr,s} - \Pi^{(y)}_{tr,s-1}),$$

which provides

$$f\left[\frac{\langle \bar{e}(\mu) \rangle_{r+1,s} - 2\langle \bar{e}(\mu) \rangle_{r,s} + \langle \bar{e}(\mu) \rangle_{r-1,s}}{d_x^2} + \frac{\langle \bar{e}(\mu) \rangle_{r,s+1} - 2\langle \bar{e}(\mu) \rangle_{r,s} + \langle \bar{e}(\mu) \rangle_{r,s-1}}{d_x^2}\right]$$
$$- 2\eta\omega \langle \bar{e}(\mu) \rangle_{r,s} = \varepsilon(\mu)_{r,s},$$

or

$$f\Delta(\mu)_{rs} - 2\eta\omega \langle \bar{e}(\mu) \rangle_{r,s} = \varepsilon(\mu)_{r,s}. \tag{10}$$

This is the error affecting, cell by cell, the thermal hypothesis and is the two-dimensional counterpart of equation (7).

The global flow error $\varepsilon(\mu)$ can be defined as

$$\varepsilon(\mu) = \frac{\sqrt{\sum_{r,s} \varepsilon^2(\mu)_{r,s}}}{\Pi_{diss}} \quad \Pi_{diss} = 2\eta\omega \sum_{r,s} \langle \bar{e}(\mu) \rangle_{r,s}.$$

The value of the proportionality coefficient f, contained in equation (10), can be determined by imposing that the global flow error over the whole structure be minimum, i.e., $\partial\varepsilon(\mu)/\partial f = 0$. A least-squares procedure leads to the following optimal value for f:

$$f_{opt} = \frac{\sum_{r,s} \Delta^2(\mu)_{r,s} \langle \bar{e}(\mu) \rangle_{r,s}}{\sum_{r,s} \Delta^2(\mu)_{r,s}}$$

This experimental value has been compared with the theoretical one given in reference [15] and a quite good agreement is found. This is, however, the value providing the best fit of energetic experimental data by the vibration conductivity hypothesis, being the equation error minimum.

In the following section, a description of the test structures and of the whole measurement chain, for the beam and the plate, is given.

7. EXPERIMENTAL SET-UP AND RESULTS

This section describes the experimental set-up and the measurement chain used in the beam and the plate tests.

In the post-processing of the experimental data, the cells corresponding to the input power point, and to the points of attachment of the test structure, were eliminated from calculations. In fact, a correct local balance equation, in correspondence to these points, requires the knowledge of both the input power and the power leaving the system through the boundaries. Especially the evaluation of this last quantity is difficult, not simply it being measurable. Thus, the evaluation of the flow error, expressed by equation (8) or equation (10), was limited to those cells (total number equal to 140) not belonging to the boundary and in which power was not injected by the excitation force.

The first set of experiments was performed on a hinging aluminium beam of length 1·4 m.

A damping layer was applied on the beam surface. Good theoretical reasons suggest avoiding very lightly damped systems. In fact, in such cases, the thermal law of propagation loses its advantages, providing an almost constant energy distribution as shown in section 5. Moreover, the damping layer introduces an important increment to the mass per unit length, but the flexural beam stiffness is not substantially modified. Therefore, the phase speed of waves decreases and, consequently, a shorter wavelength is obtained at the same excitation frequency.

The relationship between the characteristic wavelength and the circular frequency can be theoretically predicted as

$$\lambda = 2\pi \sqrt{\frac{E}{12(\rho_{in} + \rho_{dl})}} \frac{\sqrt{h}}{\sqrt{\omega}}, \tag{11}$$

where ρ_{in} and ρ_{dl} are the mass density of the metal part of the beam and the equivalent mass per unit volume due to the damping layer ($\rho_{dl} = 600\ \mathrm{kg/m^3}$) respectively.

The maximum value for μ can be estimated by $\mu_{\max} = (L/N_{\min})/\lambda$, where $N_{\min}$ and $\lambda_{\min}$ are the smallest values of the measurement stations and of the wavelength that can be used in the experimental set-up. Since $N_{\min} = 5$–6, otherwise the discussed flow error procedure becomes meaningless and $\lambda_{\min} = 7$ cm, so with the maximum corresponding frequency 10 kHz, one has $\mu_{\max} \cong (140/6)/7 \cong 3$ and the corresponding experimental μ range is $0 < \mu < 3$.

In this way, the $\langle e \rangle_i$ values can be used, as described in the previous section, to obtain the error $\varepsilon(\mu)$.

The last point concerns the evaluation of the actual μ value. Theoretically, the wavelength could be determined by relationship (11). In practice, due to the uncertainties in the parameters involved, equation (11) can provide only, a rough estimation of the characteristic wavelength. Since some relevant effects when for e.g., $d = \lambda n/4$, i.e., $\mu = n/4$, must be observed, a correct evaluation of the wavelength value in experimental conditions is important.

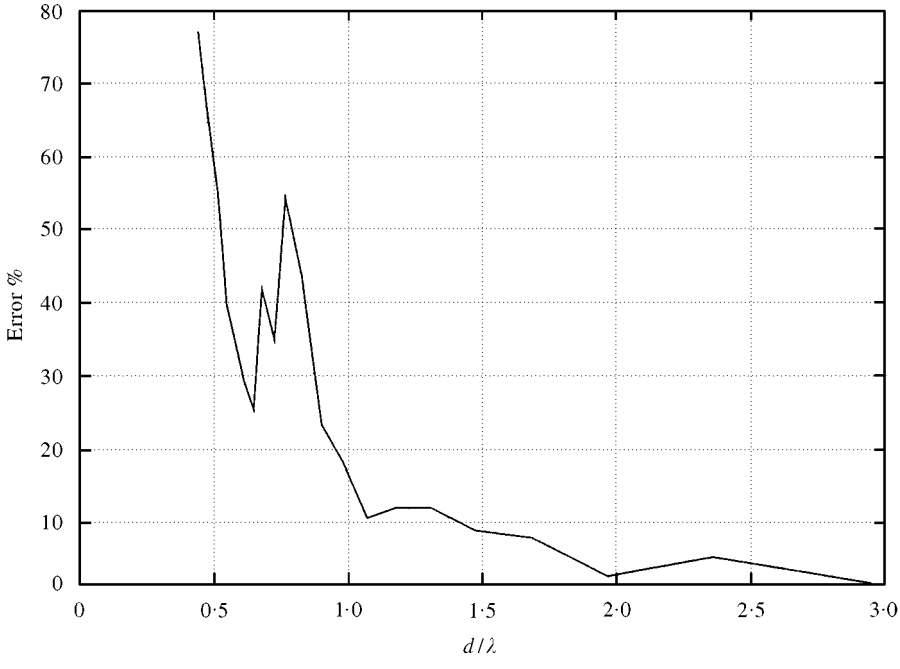

Figure 4. Beam test: equation error versus μ for harmonic excitation. Frequency 8000 Hz.

Starting from the measured space energy distribution $\langle e \rangle_i$, the discrete Fourier transform (DFT) of this sequence is computed as (limited to 128 points only) $\langle E(k_j) \rangle = DFT\{\langle e(x_i) \rangle\}$. This represents the energy distribution in the wave number domain. The location of the peak in the $\langle E \rangle_j$ sequence provides the dominant wave number k_r:

$$k_r : \langle E(k_r) \rangle \equiv \max\{\langle E(k_i) \rangle\}.$$

Since some dispersion of the energy signal around the dominant wave number is expected, a weighted average of the k's is determined as

$$\bar{k} = \frac{\sum_{l=-n}^{n} k_{r+l} \langle E \rangle_{r+l}}{\sum_{l=-n}^{n} \langle E \rangle_{r+l}} = \frac{2\pi}{\bar{\lambda}}$$

where $n = 1$–2. The previous equation provides the desired wavelength value to compute the corresponding μ.

In Figures 4 and 5 the error trend, as defined in sections 3 and 4, is plotted versus μ, at the frequency 8 kHz, and for random vibrations with a flat excitation spectrum in the range 8–10 kHz respectively.

The asymptotic limit of the error as μ increases is apparent. Moreover, the sudden decrements corresponding to the critical values $\mu = 0{\cdot}5, 1, 1{\cdot}5, 2, 3$ are also clear.

The agreement with the theory explained in the previous part of the paper seems to be very good.

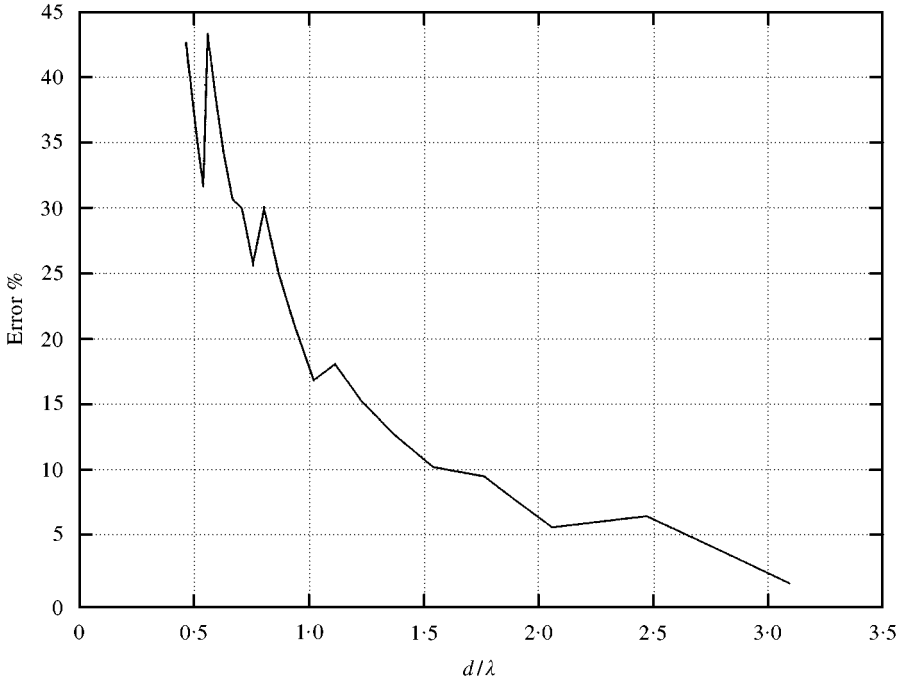

Figure 5. Beam test: equation error versus μ for random excitation. Frequency band 8000–10000 Hz.

The experimental set-up for the plate (size $0{\cdot}6 \times 0{\cdot}8\ \mathrm{m}^2$) test was analogous to that described for the beam. In this test case, the main problem did not concern the maximum frequency limit but, rather, the maximum number of measurement points.

Several practical considerations suggested using a maximum frequency of 4 kHz, with a point force applied to the plate at $x = 0{\cdot}5$, $y = 0{\cdot}5$. The minimum wavelength, determined using the DFT procedure previously discussed for the beam, was estimated to be about 4 cm. The corresponding maximum number of points in the measurement rectangular grid was $128 \times 64 = 8192$.

In Figure 6, the measured energy distribution for harmonic excitation at 4 kHz is represented by its three-dimensional graph; in Figure 7 the same representation for a random excitation in the range 3·5–4·5 kHz is shown. The energy levels are computed from the velocity laser measurements and some spurious peaks are observed, especially near the boundaries. However, they are successively eliminated and the measurement at these points is systematically repeated.

In Figures 8 and 9 the contour levels provided by the scanner laser system are plotted for the two previously mentioned cases, and the propagating wavefront is clearly identified. In Figures 10 and 11, the energy profile sections (along the longer plate side), passing through the excitation point, are shown. In the abscissa the number of the measure station along the side is represented.

The procedure described in section 7.2 was applied to produce the error parameter for the previous two test cases and the results are shown in Figures 12

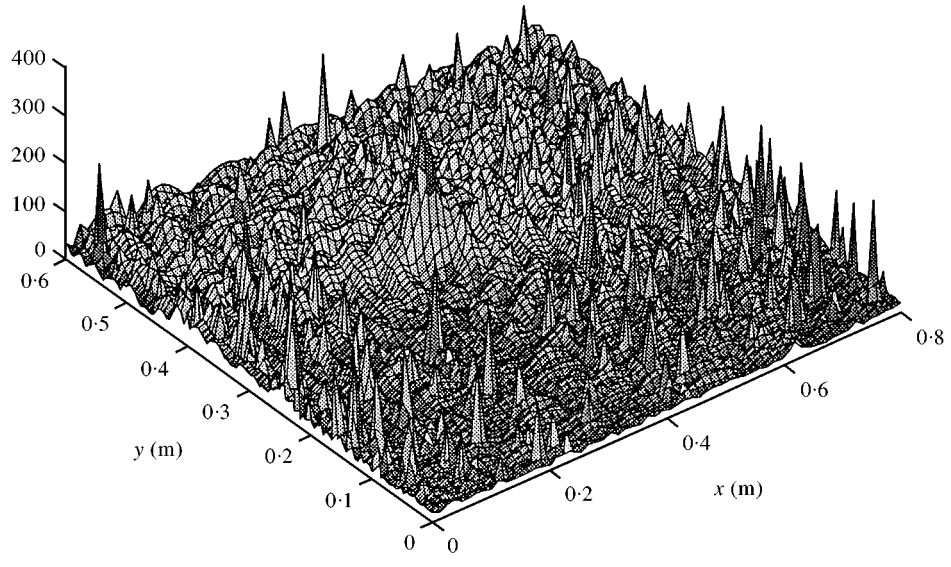

Figure 6. Plate test: energy field distribution provided by the laser head for harmonic excitation at 4000 Hz.

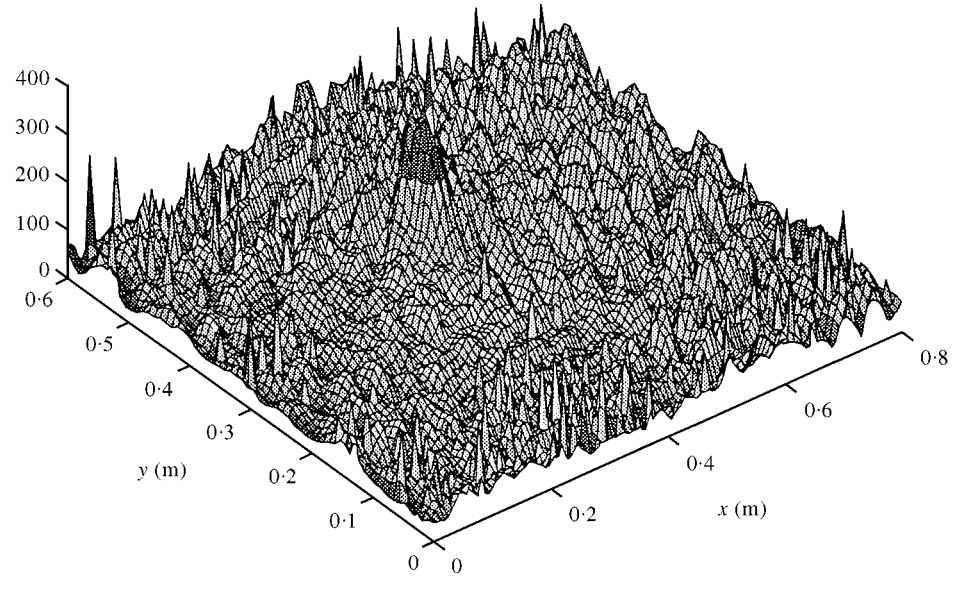

Figure 7. Plate test: energy field distribution provided by the laser head for random excitation in band 3500–4500 Hz.

and 13 respectively. Here the error equation, i.e., the power flow error, is plotted versus the μ parameter. It is clear how the power error is still very high even in the high μ range, especially for the random excitation, in accordance with the considerations presented in this paper.

The trend of the $\varepsilon(\mu)$ curves shows a behaviour of the plate energy different from that of the beam. In fact, the asymptotic limit is reached very rapidly in the beam

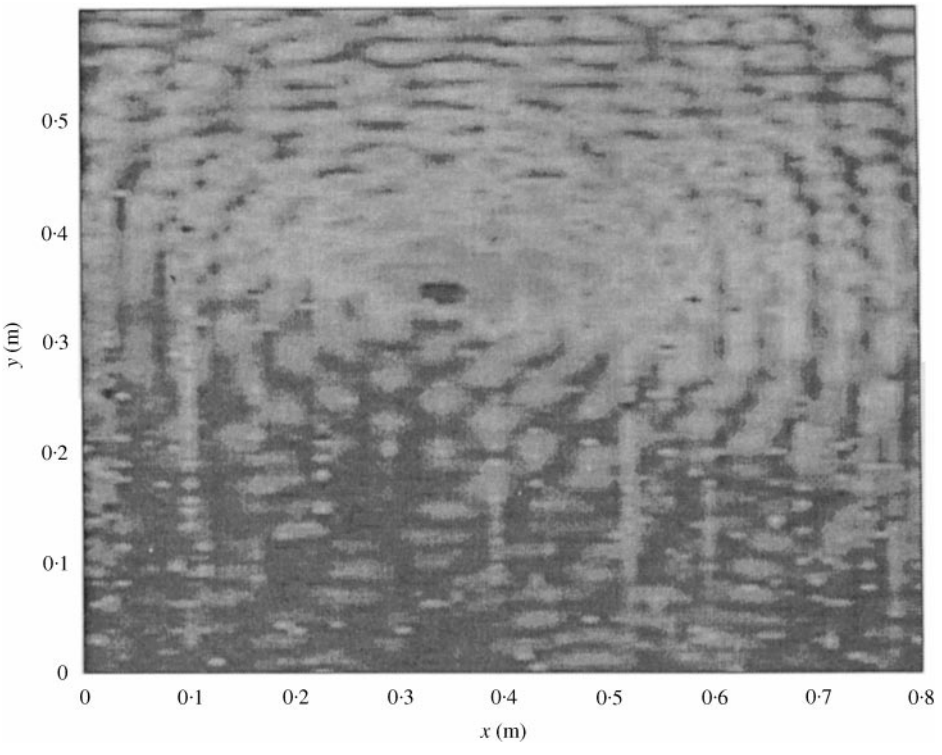

Figure 8. Plate test: computer image elaboration of the energy field over the plate surface, harmonic excitation at 4000 Hz.

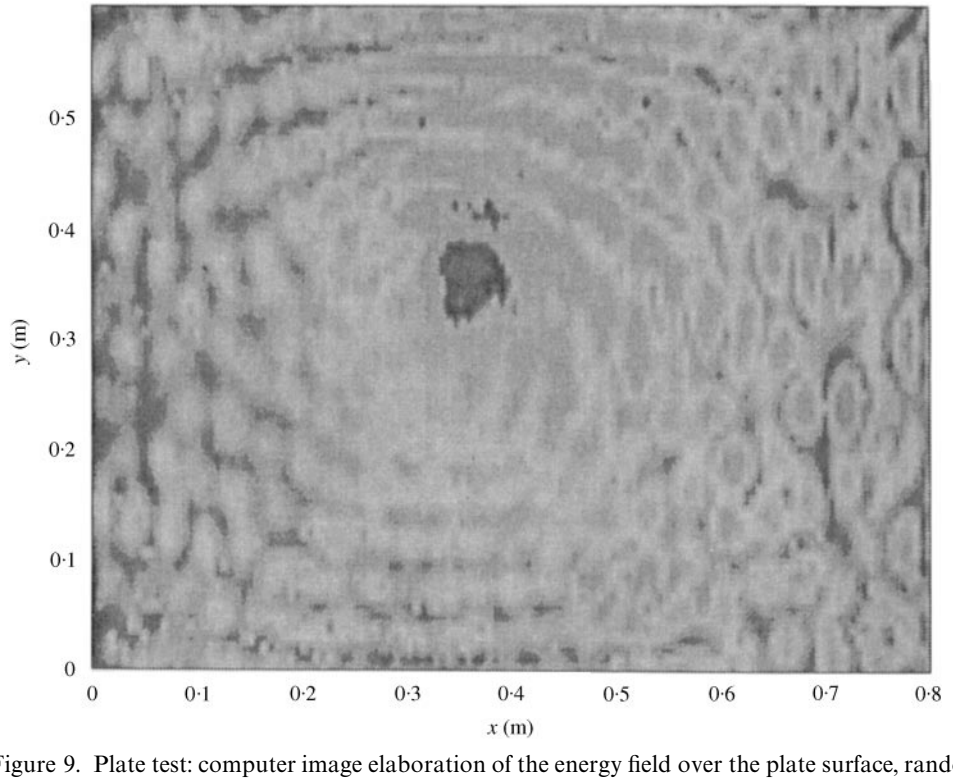

Figure 9. Plate test: computer image elaboration of the energy field over the plate surface, random excitation in band 3500–4500 Hz.

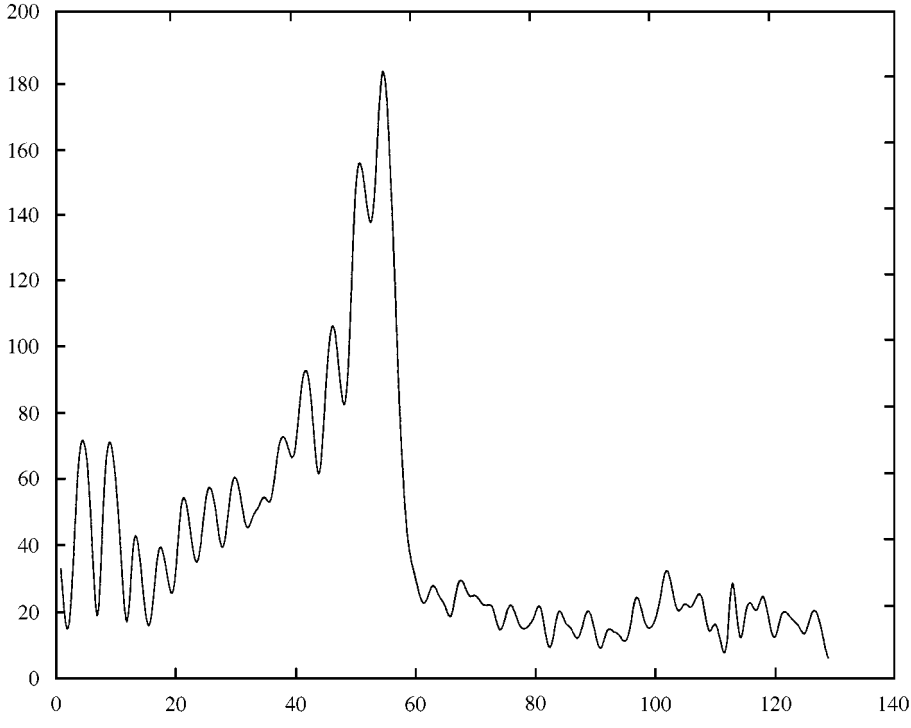

Figure 10. Plate test: energy distribution along a section, passing through the power injection point, harmonic excitation at 4000 Hz.

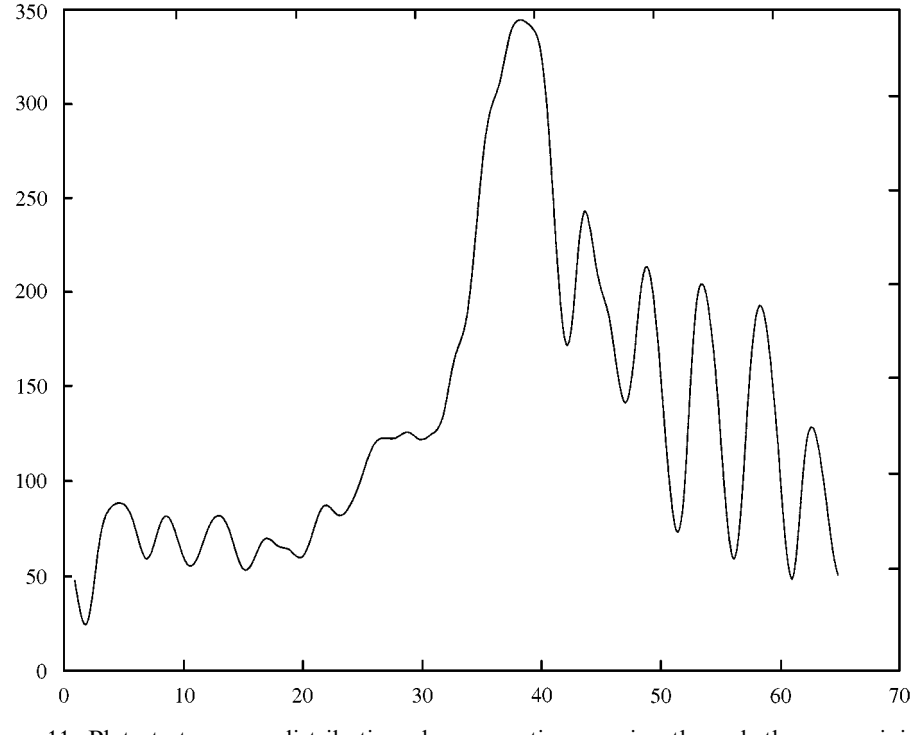

Figure 11. Plate test: energy distribution along a section, passing through the power injection point, random excitation in band 3500–4500 Hz.

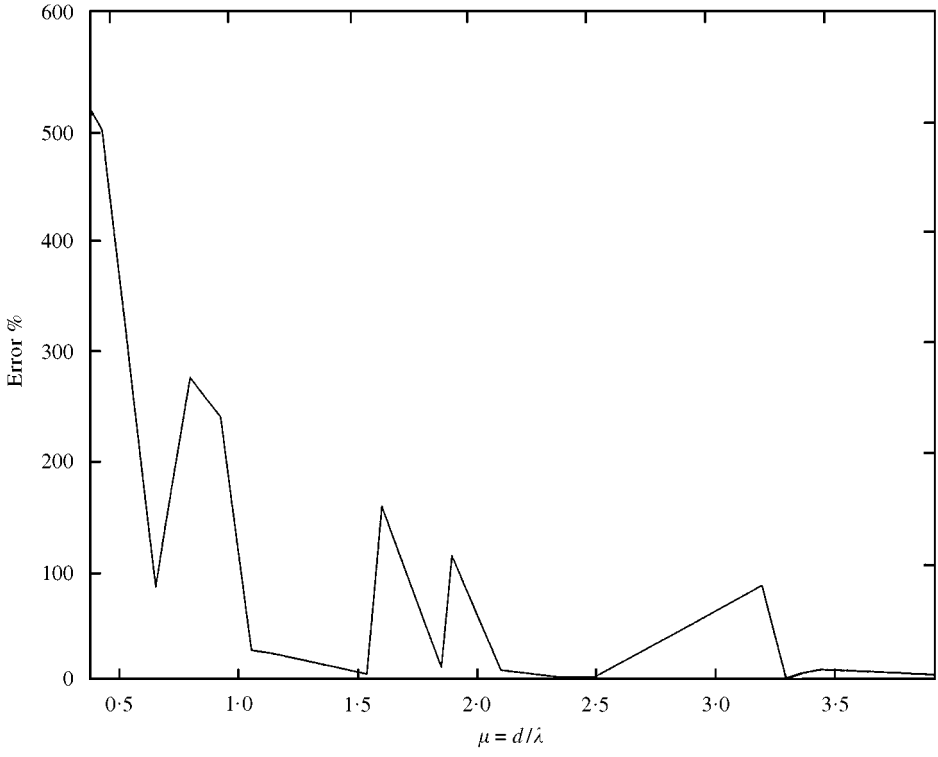

Figure 12. Plate test: equation error versus μ for harmonic excitation at 4000 Hz.

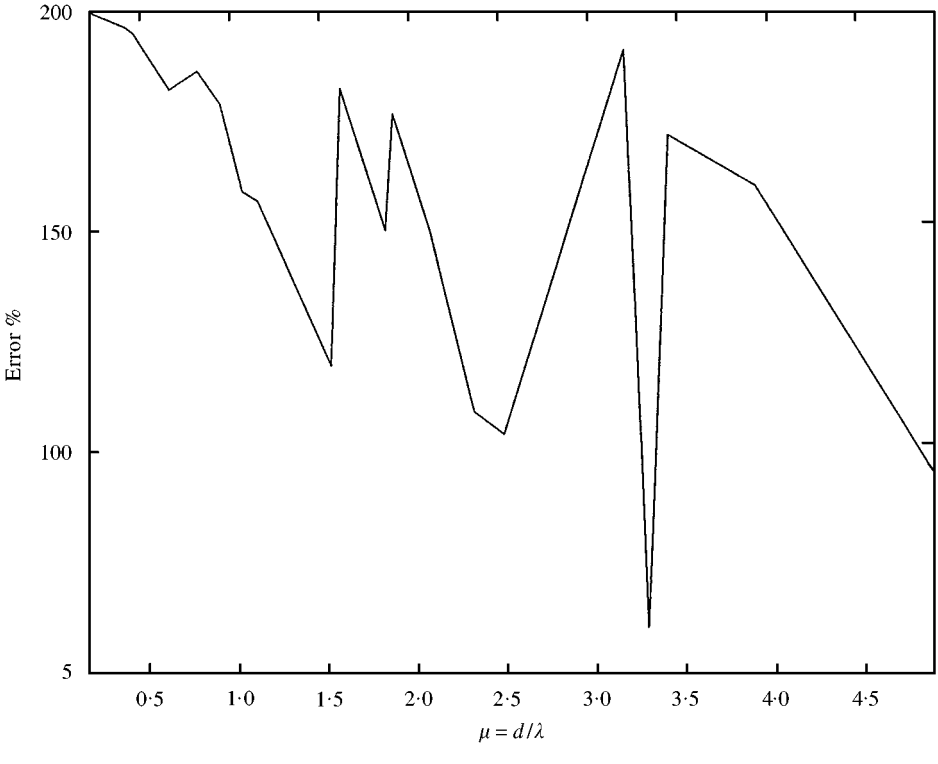

Figure 13. Plate test: equation error versus μ for random excitation in band 3500–4500 Hz.

case; on the contrary in the plate case relevant flow errors are present even when the μ parameter is appreciably high. Moreover, it is important to point out that in this last region the cell size (20 cm) approaches dimensions comparable with those of the whole plate.

These can be considered quite typical results and the comparisons between the beam and plate errors shows always this characteristic behaviour for any frequency of excitation.

8. CONCLUSIONS

In this paper a systematic theoretical and experimental analysis of the energy transfer between parts of a continuous structural system has been presented. The experiments were designed with the aim of discovering differences in the energy flow rate between one- and two-dimensional systems, as suggested by the theoretical approach developed in sections 3 and 4.

The different behaviours of the beam and of the plate are evident. The theoretical analysis explains that this difference is due to the existence of two different energy components: the coincident and the interference wave energy.

In the beam, only waves travelling in one direction are present. Thus, their mutual interaction generates only the coincident wave energy field. This component has the following basic property: an asymptotic thermal behaviour in the medium and in the large-scale range is observed; on the contrary in the small-scale range ($\mu < 1$) a non-thermal effect is still present.

The experimental results wholly confirm the theoretical analysis.

For two-dimensional systems, two energy components are simultaneously present: the coincident and the interference wave energies.

Since the first component reveals exactly the same nature of the energy met in the beam case, the second one is responsible for the different mechanism of energy propagation between one- and two-dimensional structures. The energy due to the interference between waves propagating in different directions (*iwe*), is a non-thermal contribution superimposed to the thermal one. Its presence inhibits the thermal mechanism of transmission in the medium-scale range, where the non-thermal component has the same order of magnitude as that of the thermal one. In this case, the non-thermal behaviour persists up to higher values of the scale factor, depending on the loss coefficient (section 5). Therefore, for plates the following mechanism of transmission is revealed: a non-thermal behaviour in the small- and medium-scale range is observed. In the large-scale range the thermal behaviour is slowly increased; however this asymptotic tendency shows that the non-thermal component is largely dominant in the whole medium-scale range; moreover, for random excitation, no significant flow error reduction is observed, even in the high scale range.

The theoretical results seem to match the experimental evidence very satisfactorily, especially when the beam is compared with the plate.

The analysis developed is in agreement with some results obtained in reference [29, 37], where an interesting check of the thermal power flow analysis was carried

out for a beam and a complex structure similar to a stiffened plate. The beam case matches very well the thermal power flow prediction, while, in the second case, the authors found a relevant discrepancy between theoretical prediction and measurements.

About the applicability of the thermal analogy to the analysis of two- and three-dimensional structures, the feeling of the authors is that an alternative constitutive energy relationship must be investigated. Although the intuition contained in the thermal analogy is fascinating, it is likely that the thermal power flow takes into account only a first order contribution of a more complicated phenomenon.

ACKNOWLEDGMENTS

The authors express their thanks to Professor Aldo Sestieri for his support, suggestions and encouragement in developing this work.

An acknowledgement to Professor Tomasini for his kindness in making available the scanning laser system of the Department of Mechanics of the University of Ancona, and to Dr. Pisoni and Eng. Santolini for their effective technical support in performing the laser measurements on the plate tested in the present paper.

This work was also supported by the Italian of Merchant Navy, in the frame of the INSEAN (Italian Ship Model Basin) research program 1991–1993.

REFERENCES

1. F. J. Fahy and A. D. Mohammed 1992 *Journal of Sound and Vibration* **158**, 45–67. A study of uncertainty in applications of SEA to coupled beam and plate systems, Part I: computational experiments.
2. E. Rebillard and J. L. Guyader 1995 *Journal of Sound and Vibration* **188**, 435–454. Vibrational behaviour of a population of coupled plates: hypersensitivity to the connection angle.
3. R. A. Ibrahim 1987 *Applied Mechanics Review* **40**, 309–328. Structural dynamics with parameter uncertainties.
4. R. H. Lyon 1975 *Statistical Energy Analysis of Dynamical Systems, Theory and Applications*. MA, U.S.A.: MIT Press.
5. F. J. Fahy and De Yuan Yao 1987 *Journal of Sound and Vibration* **114**, 1–11. Power flow between non-conservatively coupled oscillators.
6. J. Woodhouse 1981 *Journal of Acoustical Society of America* **69**, 1695–1709. An approach to the theoretical background of the statistical energy analysis applied to structural vibration.
7. G. Maidanik and J. Dickey 1990 *Journal of Sound and Vibration* **139**, 31–42. Wave derivation of the energetics of driven coupled one-dimensional dynamic systems.
8. A. J. Keane and W. G. Price *Proceedings of the Royal Society of London A* **436**, 537–568. Energy flows between arbitrary configurations of conservatively-coupled multi-modal elastic subsystems.
9. R. S. Langley 1989 *Journal of Sound and Vibration* **135**, 499–508. A general derivation of the statistical energy analysis equations for coupled dynamic systems.
10. B. R. Mace 1994 *Journal of Sound and Vibration* **178**, 95–112. On the statistical energy analysis hypothesis of coupling power proportionality and some implications of its failure.

11. Y. KISHIMOTO and D. BERNSTEIN 1995 *Journal of Sound and Vibration* **182**, 23–58. Thermodynamic modelling of interconnected systems. Part I: conservative coupling.
12. Y. KISHIMOTO and D. BERNSTEIN 1995 *Journal of Sound and Vibration* **182**, 59–76. Thermodynamic modelling of interconnected systems. Part II: conservative coupling.
13. V. D. BELOV, S. A. RYBAK and B. D. TARTAKOVSKII 1977 *Soviet Physics Acoustics* **23**. Propagation of vibrational energy in absorbing structures.
14. L. E. BUVAILO and A. V. IONOV 1980 *Soviet Physics Acoustics* **26**, 277–289. Application of the finite element method to the investigation of the vibroacoustical characteristics of structures at audio frequencies.
15. D. J. NEFSKE and S. H. SUNG 1989 *Journal Vibration, Acoustics, Stress and Reliability in Design* **111**, 94–100. Power flow finite element analysis of dynamic systems: theory and application to beams.
16. R. S. LANGLEY 1992 *Journal of Sound and Vibration* **159**, 483–502. A wave intensity technique for the analysis of high frequency vibrations.
17. A. LE BOT and L. JEZEQUEL 1993 *Proceedings of the Institute of Acoustics* **15**, 561–568. Energy formulation for one dimensional problems.
18. A. LE BOT 1994 *Ph.D. Thesis, L'Ecole Centrale de Lyon*. Equations énergetiques en mécanique vibratoire. Application au domaine des moyennes et hautes fréquences.
19. M. N. ICHCHOU and L. JEZEQUEL 1995 *Proceedings of the Inter Noise, Newport Beach*. A general propagative approach for the energy flow models and the heat conduction analogy of one-dimensional systems.
20. A. CARCATERRA 1995 *Ph.D. Thesis, Università di Roma 'La Sapienza'*. Risposta dinamica di inviluppo: una nuova formulazione per problemi dinamici ad alta frequenza.
21. A. CARCATERRA and A. SESTIERI 1995 *Proceedings of the 11th International Modal Analysis Conference, Nashville (Tennesee)*. 370–376. Envelope versus envelope-phase model for high frequency structural problems.
22. A. SESTIERI and A. CARCATERRA 1996 *Journal of Sound and Vibration* **187**, 283–295. An envelope energy model for high frequency dynamic structures.
23. A. CARCATERRA and A. SESTIERI 1997 *Journal of Sound and Vibration* **188**, 205–233. Complex envelope displacement analysis: a quasi-static approach to vibrations.
24. J. C. WOHLEVER and R. J. BERNHARD 1992 *Journal of Sound and Vibration* **153**, 1–19. Mechanical energy flow models in rods and beams.
25. R. S. LANGLEY 1995 *Journal of Sound and Vibration* **182**, 637–657. On the vibrational conductivity approach to high frequency dynamics for two-dimensional structural components.
26. A. CARCATERRA and A. SESTIERI 1995 *Journal of Sound and Vibration* **188**, 269–282. Energy density equations and power flow in structures.
27. M. N. ICHCHOU and L. JEZEQUEL 1996 *Journal of Sound and Vibration* **195**, 679–685. Comments on simple models of the energy flow in vibrating membranes and on simple models of the energetics of transversely vibrating plates.
28. M. DJIMADOUM and J. L. GUYADER 1993 *Proceedings of the 4th International Congress on Intensity Techniques, Senlis (France)*, 379–386. Prediction of coupled beam energy with equations of diffusion—boundary, excitation and coupling conditions.
29. J. T. XING and W. G. PRICE 1999 *Proceedings of the Royal Society of London A* **455**, 401–436. A power-flow analysis based on continuum dynamics.
30. D. J. PALMER, E. J. WILLIAMS and H. J. FOX 1993 *Proceedings of the 4th International Congress on Intensity Techniques, Senlis (France)*, 313–322. Energy flow analysis in built-up structures.
31. R. J. BERNHARD and P. CHO 1993 *Proceedings of the 4th International Congress on Intensity Techniques, Senlis (France)*, 445–448. Energy flow analysis of a light truck frame: a verification study.
32. P. M. MORSE and H. FESHBACH 1953 *Methods of Theoretical Physics*. New York: McGraw-Hill.

33. L. CREMER, M. HECKL and E. E. UNGAR 1988 *Structure-Borne Sound*. Berlin: Springer-Verlag.
34. A. CARCATERRA 1998 *IUTAM Symposium on Statistical Energy Analysis (F. J. Fahy and W. G. Price) Southampton, UK*. Dordrecht: Kluwer. Wavelength scale effects on energy propagation in structures.
35. A. CARCATERRA and A. SESTIERI 1994 *Proceedings of the 5th International Conference on Recent Advances in Structural Dynamics*, Southampton, U.K., 482–493. Energy trend in high frequency structural problems.
36. R. COURANT and D. HILBERT 1962 Methods of Mathematical Physics, Vol. II. U.S.A.: Interscience publishers, John Wiley & Sons.
37. PALMER, H. J. FOX and E. J. WILLIAMS 1994 *Proceedings of the 5th International Conference on Recent Advances in Structural Dynamics, Southampton, U.K.*, 472–481. Application of the energy flow approach to vibrational analysis of real structures.

APPENDIX A

The expression for the flow error is found by using equation (1):

$$\langle \bar{e} \rangle = \kappa_e \left[\left(\frac{e^{\pi\mu\eta} - 1}{\pi\mu\eta e^{\pi\mu(\eta/2)}} \right) \cdot (a e^{-k_B(\eta/2)x} + b e^{k_B(\eta/2)x}) + c \left(\frac{\sin(2\pi\mu)}{2\pi\mu} \right) \cos(2k_B x + \varphi) \right]$$

$$= \langle \bar{e} \rangle_t + \langle \bar{e} \rangle_d, \qquad \kappa_e = \frac{1}{2} \rho A \omega^2.$$

Assume, for the sake of simplicity,

$$\bar{E}_i = \langle \bar{e}(x_i) \rangle = \kappa_e \left[\left(\frac{e^{\pi\mu\eta} - 1}{\pi\mu\eta e^{\pi\mu(\eta/2)}} \right) (a e^{-k_B(\eta/2)x_i} + b e^{k_B(\eta/2)x_i}) + c \left(\frac{\sin(2\pi\mu)}{2\pi\mu} \right) \cos(2k_B x_i + \varphi) \right],$$

$$\bar{E}_i = \alpha(\mu)(a e^{-k_B(\eta/2)x_i} + b e^{k_B(\eta/2)x_i}) + \beta(\mu)\cos(2k_B x_i + \varphi).$$

By the Euler's formula, since $x_{i\pm1} = x_i \pm d$, one has

$$\bar{E}_{i\pm1} = \alpha(\mu)(a e^{-k_B(\eta/2)x_i} e^{\mp k_B(\eta/2)d} + b e^{k_B(\eta/2)x_i} e^{\pm k_B(\eta/2)d}) + \frac{\beta(\mu)}{2} (e^{-j\varphi} e^{-2jk_B x_i} e^{\mp 2jk_B d} + e^{j\varphi} e^{2jk_B x_i} e^{\pm 2jk_B d}),$$

Thus

$$\bar{E}_{i+1} - 2\bar{E}_i + \bar{E}_{i-1} = \alpha(\mu)(e^{k_B(\eta/2)d} + e^{-k_B(\eta/2)d} - 2)(a e^{-k_B(\eta/2)x_i} + b e^{k_B(\eta/2)x_i}) + \frac{\beta(\mu)}{2} (e^{2jk_B d} + e^{-2jk_B d} - 2)(e^{-j\varphi} e^{-2jk_B x_i} + e^{j\varphi} e^{2jk_B x_i}).$$

The power flow error, defined by equation (7), assumes therefore the form

$$\alpha(\mu)(a e^{-k_B(\eta/2)x_i} + b e^{k_B(\eta/2)x_i}) \left[f \frac{(e^{k_B(\eta/2)d} + e^{-k_B(\eta/2)d} - 2)}{d^2} - 2\eta\omega \right]$$

$$+\frac{\beta(\mu)}{2}\left(\mathrm{e}^{-\mathrm{j}\varphi}\mathrm{e}^{-2\mathrm{j}k_B x_i}+\mathrm{e}^{\mathrm{j}\varphi}\mathrm{e}^{2\mathrm{j}k_B x_i}\right)\left[f\,\frac{(\mathrm{e}^{2\mathrm{j}k_B d}+\mathrm{e}^{-2\mathrm{j}k_B d}-2)}{d^2}-2\eta\omega\right]=\varepsilon_i \quad \text{(A1)}$$

In the present analysis the constant f is determined through the least-square procedure described in section 4. However, it can be numerically verified that this value is approximately given by $f \approx 8\omega/k_B^2\eta$, with the data considered in the experimental case. Thus one has

$$f\,\frac{(\mathrm{e}^{k_B(\eta/2)d}+\mathrm{e}^{-k_B(\eta/2)d}-2)}{d^2}-2\eta\omega \approx \frac{8\omega}{k_B^2\eta}\,\frac{(\mathrm{e}^{k_B(\eta/2)d}+\mathrm{e}^{-k_B(\eta/2)d}-2)}{d^2}-2\eta\omega$$

$$=\left[\frac{(\mathrm{e}^{\pi\mu\eta}+\mathrm{e}^{-\pi\mu\eta}-2)}{(\pi\mu\eta)^2}-1\right]2\eta\omega \approx 0$$

The last relationship is easily determined once a Taylor expansion up to the second order in terms of η of $e^{\pi\mu\eta}+e^{-\pi\mu\eta}-2$ is performed (the damping factor is actually small, i.e. $\eta = 0{\cdot}05 \div 0{\cdot}1$). Therefore, by substitution of the last relationship in equation (A1), equation (8) is obtained:

$$\beta(\mu)\cos(2k_B x_i+\varphi)\left[\frac{2(\cos 4\pi\mu-1)}{(\pi\mu\eta)^2}-1\right]2\eta\omega=\varepsilon_i.$$